

AD-A055 123

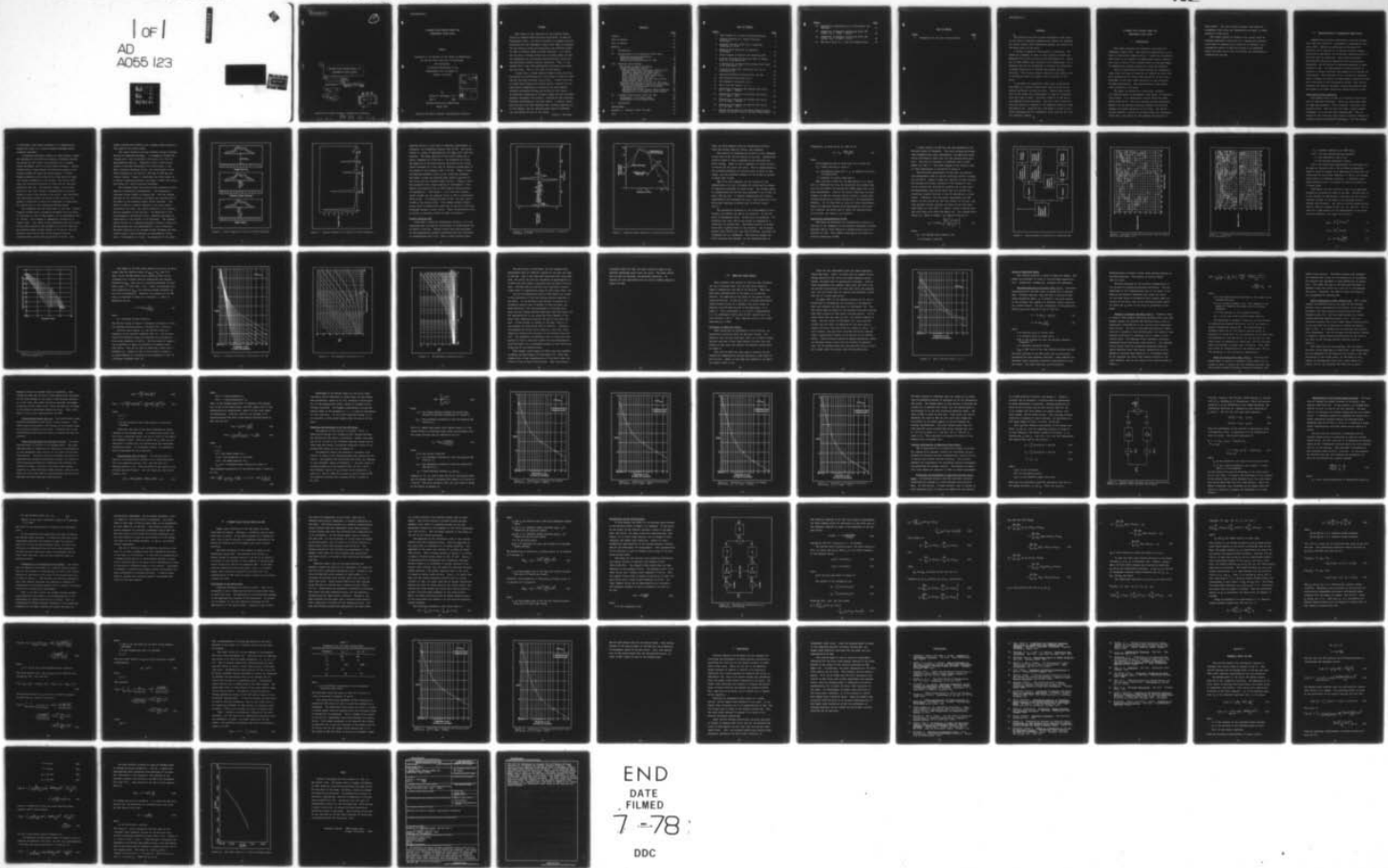
AIR FORCE INST OF TECH WRIGHT-PATTERSON AFB OHIO SCH--ETC F/G 20/14
A RANDOM POINT PROCESS MODEL FOR ATMOSPHERIC RADIO NOISE.(U)

MAR 78 S D HETTINGER
AFIT/GE/EE/78-3

UNCLASSIFIED

NL

1 OF 1
AD
A055 123



END
DATE
FILMED
7-78
DDC

14

AFIT/GE/EE/78-3



6

A RANDOM POINT PROCESS MODEL FOR
ATMOSPHERIC RADIO NOISE.

9

master's THESIS,

10

AFIT/GE/EE/78-3

Steven D./Hettinger
2nd Lt USAF

11

Mar 78

12

88 p.

DDC
RECEIVED
JUN 16 1978
AYE

Approved for public release; distribution unlimited

012 225 78 06 13 040

act

A RANDOM POINT PROCESS MODEL FOR
ATMOSPHERIC RADIO NOISE

THESIS

Presented to the Faculty of the School of Engineering
of the Air Force Institute of Technology
Air University
in Partial Fulfillment of the
Requirements for the Degree of
Master of Science

by

Steven D. Hettinger, B.S.

2nd Lt

USAF

Graduate Electrical Engineering

March 1978

ACCESSION for	
NTIS	White Section <input checked="" type="checkbox"/>
DDC	Buff Section <input type="checkbox"/>
UNANNOUNCED	<input type="checkbox"/>
JUSTIFICATION.....	
BY.....	
DISTRIBUTION/AVAILABILITY CODES	
Dist.	AVAIL. and/or SPECIAL
A	

Preface

This thesis is the outgrowth of two previous theses written by Kenneth Olson and Allen Nejezchleb, by Rome Air Development Center, and from an interest in optimal receiver structures for the atmospheric radio noise (ARN) environment. The two theses by Olson and Nejezchleb used existing models for ARN to evaluate CPFSK and CFSK receivers. As a result of this work it became obvious that existing models for ARN are inadequate for evaluating existing receiver structures and specifying optimal receiver structures. Thus, it was decided that a new, more analytically tractable noise model must be found. That is the topic of this thesis.

I would like to thank Captains Kenneth Olson and Allen Nejezchleb for introducing me to the subject of ARN and their patient help when starting this project. I would also like to thank Peter Maybeck and Captain Stanley Robinson for the many helpful suggestions on technical and non-technical problems encountered during the writing of this thesis. I am especially appreciative of Major Joseph Carl who provided guidance throughout this project, steering me away from many problems and helping me over many others. A special thanks must also go to my wife Katherine who, besides composing all of the figures, gave me constant moral support throughout the nine months of work on the thesis.

Steven D. Hettinger

Contents

	<u>Page</u>
Preface	ii
List of Figures	iv
List of Tables	vi
Abstract	vii
I. Introduction	1
II. Characteristics of Atmospheric Radio Noise	3
Lightning Discharge Mechanism	3
Factors Affecting ARN	8
Statistical Characteristics of ARN	12
III. Empirical Noise Models	25
Philosophy of Empirical Models	25
Survey of Empirical Models	28
APD Representation by Crichlow (Refs 5;6;7)	28
Beckman's Lognormal APD Model (Ref 3)	29
Beach and George Noise Model (Ref 2)	30
Hall's Generalized t Model (Refs 12;24)	31
M-Distribution Model (Ref 18)	32
Power Rayleigh Model for ARN (Ref 8:83-87)	32
Mixture Model (Ref 24:38-43)	33
Measuring the Exactness of Fit for APD Curves	35
Inherent Deficiencies of Empirical Noise Models	41
Evaluating the Performance of Existing Receiver Structures	41
Specification of the Optimal Binary Receiver	45
Inadequacies of the Empirical Noise Models	46
IV. A Random Point Process Model for ARN	48
Development of the Noise Model	48
Verification of the Process Model	52
V. Conclusions	67
Bibliography	69
Appendix A: Beckman's Model for ARN	72
Vita	77

List of Figures

<u>Figure</u>		<u>Page</u>
1	Three Stages of a Cloud-to-Ground Discharge . . .	6
2	Current Waveform of a Typical Multiple Discharge	7
3	Measured Electric Field from a Lightning Discharge at 20 Km	9
4	Measured Power Spectrum of Lightning Discharges	10
5	Block Diagram of Receiver for Measuring ARN . . .	14
6	Location of Receiving Stations Used to Compile Data for CCIR Report 322	15
7	A Typical Plot of World-Wide Average Noise Power as in CCIR Report 322	16
8	A Typical Noise Power Conversion Plot as in CCIR Report 322	18
9	Measured-Probability Distribution for ARN	20
10	APD Bandwidth Conversion Plot 1	21
11	APD Bandwidth Conversion Plot 2	22
12	Short Term APD Curves, $V_d = 4$	27
13	Comparison of Measured and Beckman APD Curves, $V_d = 4$ (MSE = .00924)	37
14	Comparison of Measured and Mixture APD Curves, $V_d = 4$ (MSE = .081)	38
15	Comparison of Measured and Beckman APD Curves, $V_d = 10$ (MSE = .00146)	39
16	Comparison of Measured and Mixture APD Curves, $V_d = 10$ (MSE = .347)	40
17	Optimal Binary Receiver for White Gaussian Noise, Signals are Equally Likely and Have Equal Energy	43

<u>Figure</u>		<u>Page</u>
18	Mathematical Representation of CCIR Report 322 Receiver	53
19	Comparison of Measured and Process Model APD Curves, $V_d = 4$ (MSE = .00958)	64
20	Comparison of Measured and Process Model APD Curves, $V_d = 10$ (MSE = .0357)	65
21	APD Curve Slope vs. σ from the Beckman Model	76

List of Tables

<u>Table</u>		<u>Page</u>
I	Parameters for the Point Process Model	63

Abstract

The physical processes causing atmospheric radio noise in the very-low frequency communication channel are examined. The return strokes from lightning discharges are found to be the major source of the noise.

A survey of empirical noise models is presented. The models are compared in terms of their ability to match the measured first order statistics from CCIR Report 322. While all of these models have advantages and disadvantages, it is observed that all are inadequate to evaluate the performance of known receivers or to specify the optimal receiver structure. This results because empirical noise models give no information about the higher order statistics of the noise.

A new model for atmospheric radio noise is developed. This model is a random process model that is based on the physical processes causing the noise. Higher order statistics of the noise can be determined, at least in principle, from this type of model. The model consists of the sum of two compound Poisson processes. The first order statistics from this model are compared to the measured statistics from CCIR Report 322. Based on this, the model is found to be a valid representation for atmospheric radio noise in the very-low frequency channel.

A RANDOM POINT PROCESS MODEL FOR
ATMOSPHERIC RADIO NOISE

I. Introduction

This report proposes and evaluates a new model for atmospheric radio noise. This model has applications in the field of statistical communications. A model for atmospheric radio noise is of interest in communication theory, because this type of noise is the limiting factor on the performance of communication systems operating at very-low frequency.

There are many models already existing for atmospheric radio noise, but most of these are of limited use since they only characterize the first order statistics of the noise. Knowledge of the first order statistics is not sufficient for many applications. The proposed model allows higher order statistics to be found.

The report is divided into three major sections: (1) characteristics of atmospheric radio noise, (2) empirical noise models, (3) a random point process model for atmospheric radio noise. The first section provides background material on the physical processes causing the noise and presents the known statistics of the noise. The second section presents a survey of existing models for atmospheric radio noise, and points out the inherent deficiencies of

these models. The last section proposes a new model for atmospheric radio noise and demonstrates the model is representative of the noise.

This report should be thought of as a pilot study on modeling atmospheric radio noise as a random point process. A new model is proposed and is shown to be feasible, but a considerable amount of work still needs to be performed before the model can be used to evaluate the performance of communication systems.

II. Characteristics of Atmospheric Radio Noise

Communication receivers operating at very-low frequencies (VLF) are limited in performance by atmospheric radio noise (ARN). Before the performance of existing VLF receivers can be analyzed or an optimal receiver configuration can be specified, the statistical characteristics of the noise must be understood. The physical processes affecting ARN include the generating and the propagation mechanisms, and the effects of measuring equipment on measurements of ARN. An understanding of these processes is required to analyze existing noise models and to develop new noise models. The discussion of the statistical characteristics includes the results of measurements conducted on ARN, and a discussion of the stationarity of ARN. This section discusses the physical processes causing and affecting ARN, and presents the known statistical characteristics of ARN.

Lightning Discharge Mechanism

The primary source of ARN is the electric field generated by lightning discharges. There are three major types of lightning discharge: cloud-to-ground, intracloud, and cloud-to-cloud. Only the first of these, cloud-to-ground discharge, is of interest when examining ARN. This is because of the relatively weak electric currents involved in cloud-to-cloud and intracloud discharges. For the purpose

of this paper, any future references to a lightning discharge will refer to a cloud-to-ground discharge unless otherwise specified.

A lightning discharge consists of three separate stages: the building of an electrical potential difference between the ground and the cloud, the occurrence of a streamer-leader discharge, and of a return stroke discharge. During thunderstorms, clouds acquire an electrical potential difference between the upper and lower surface. Positive charge accumulates at the top of the cloud while the negative charge accumulates at the bottom. The factors that cause the electrical potential to build are not currently understood (Ref 28). The negative charge, in the lower portion of the cloud, causes a concentration of positive charge to form on the surface of the earth. When the potential difference between the bottom of the cloud and the ground is sufficient to cause the atmosphere to break down, the second stage of the lightning discharge begins.

The atmosphere does not break down in one step. Instead, slightly ionized paths (streamers) propagate from the cloud to the ground in 10m to 100m segments, at an approximate rate of $.5\text{m}/\mu\text{sec}$. The streamer is immediately followed by a leader stroke. The leader stroke propagates down the already ionized path created by the streamer at a rate of $70\text{m}/\mu\text{sec}$. The streamer-leader process repeats at 25 μsec to 100 μsec intervals until one or more of the branches from the streamer-leader reaches the ground (Ref 11:15-18). The

highly ionized path formed by the streamer-leader process is then used by the return stroke.

The return stroke is the most powerful stroke occurring during the lightning discharge. It propagates through the ionized path, from the ground to the cloud, at a rate of approximately $80\text{m}/\mu\text{sec}$. Frequently three or four return strokes (a multiple discharge) will occur within .2 sec. When a multiple discharge occurs, the ionized path is kept from collapsing by the flow of a 500 amp to 1000 amp continuous current. Figure 1 illustrates the three stages of a typical lightning discharge, and Figure 2 shows the current and timing of a typical multiple discharge.

The streamer-leader and return strokes generate electromagnetic interference (atmospherics). The atmospherics from many storms combine to produce ARN. The time varying waveform of the interference determines the distribution of the power in the frequency domain (power spectrum). The effect of ARN on a receiver depends on the power density spectrum of the noise, the center frequency of the receiver, and the bandwidth of the receiver. The magnitude of the electromagnetic interference from a lightning discharge is proportional to the current of the discharge. The streamer-leader portion of a lightning discharge contains a series of 300 amp pulses that are approximately $1\ \mu\text{sec}$ in duration. The power spectrum of the streamer-leader discharge has been found to have a center frequency of approximately 30 KHz, and a 3 db bandwidth of 40 KHz. The magnitude of the power

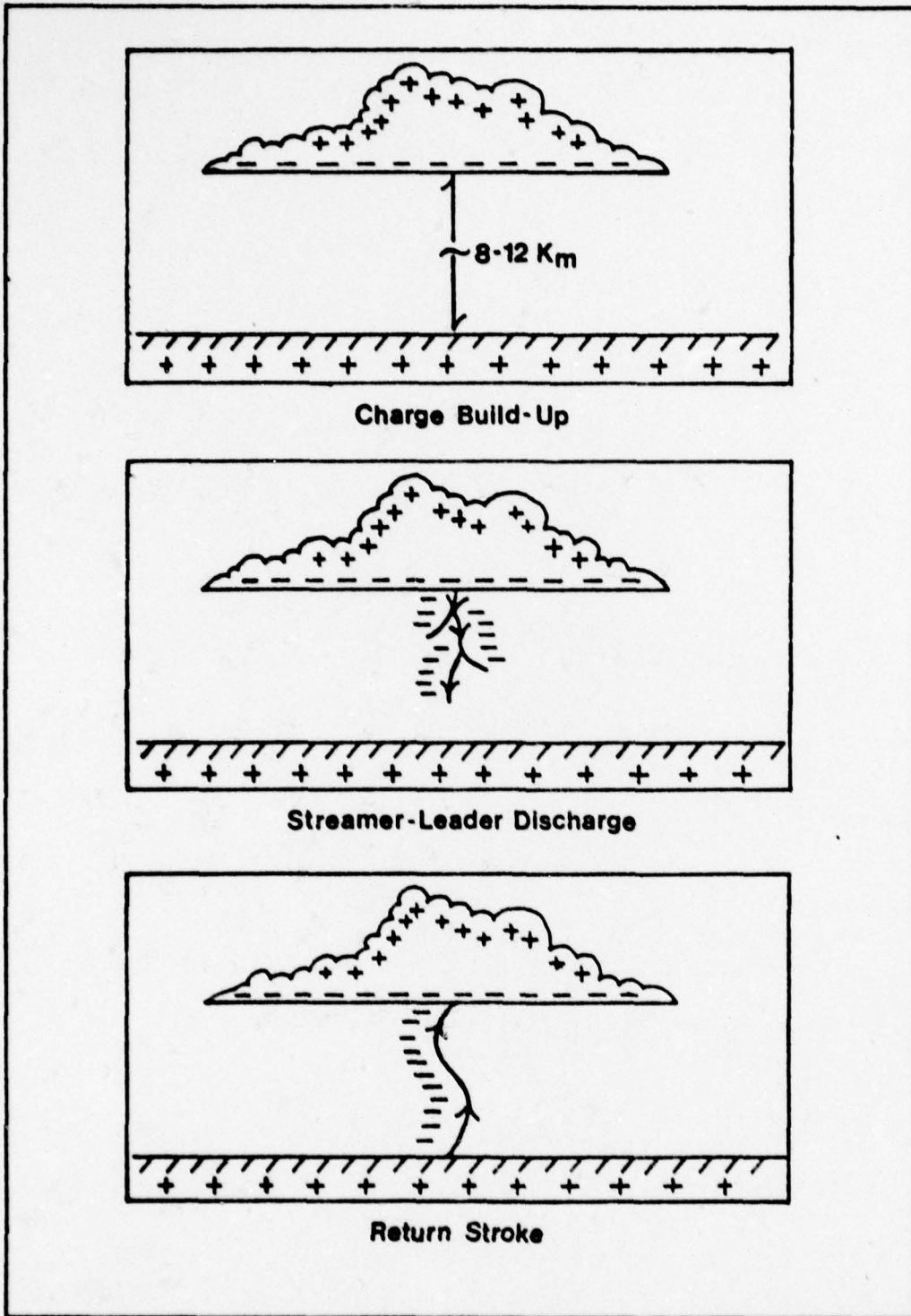


Figure 1. Three Stages of a Cloud-to-Ground Discharge

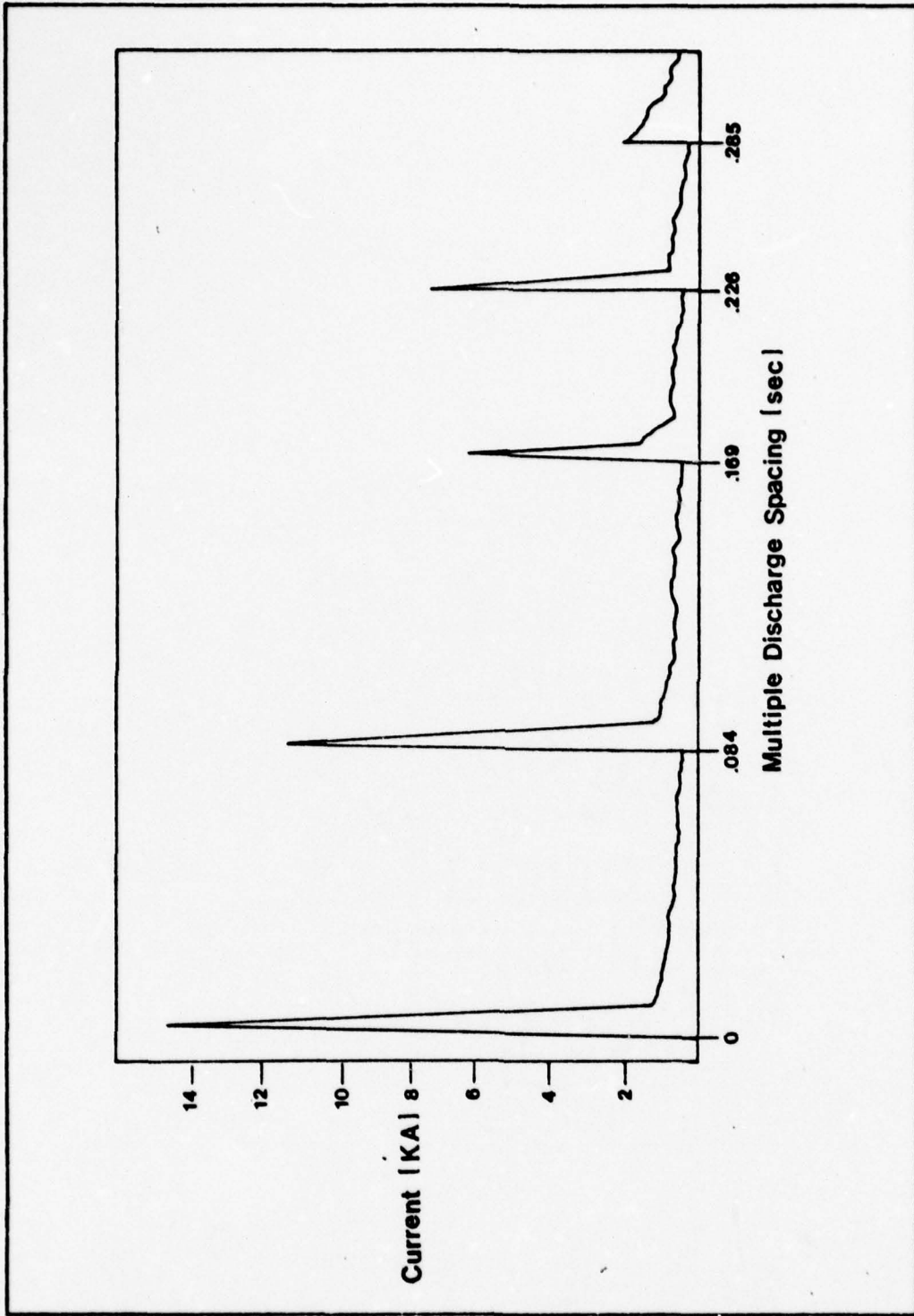


Figure 2. Current Waveform of a Typical Multiple Discharge

spectrum falls at a rate that is inversely proportional to frequency, for frequencies greater than 40 KHz. The return stroke is a pulse of approximately 20 k-amps with a 100 μ sec duration. The power spectrum of the return stroke has a center frequency of 10 KHz and a 3 db bandwidth of 10 KHz. The magnitude of the power density spectrum for the return strike decreases at a rate that is inversely proportional to the square of the frequency (Ref 11:19-20). Figure 3 shows the measured waveform from an actual lightning discharge, and Figure 4 shows the measured power density spectrum of the return and the streamer-leader strokes. Figures 3 and 4 were produced from a small sampling of atmospherics; these figures are presented only to show general characteristics of atmospherics. From Figure 4, it is seen the streamer-leader strokes are the dominant source of ARN at frequencies above 60 KHz. At frequencies below 30 KHz, the main source of ARN is the return stroke. The streamer-leader strokes always occur in groups while there may or may not be multiple discharges during a return stroke. These characteristics will be useful in deriving a model for ARN in section IV.

Factors Affecting ARN

Since ARN is caused by thunderstorm activity, it is not surprising that the spatial distribution of thunderstorms has an effect on the ARN. Several studies have been performed to find geographical patterns associated with the occurrence of thunderstorms (Ref 4:31). Both of these studies found

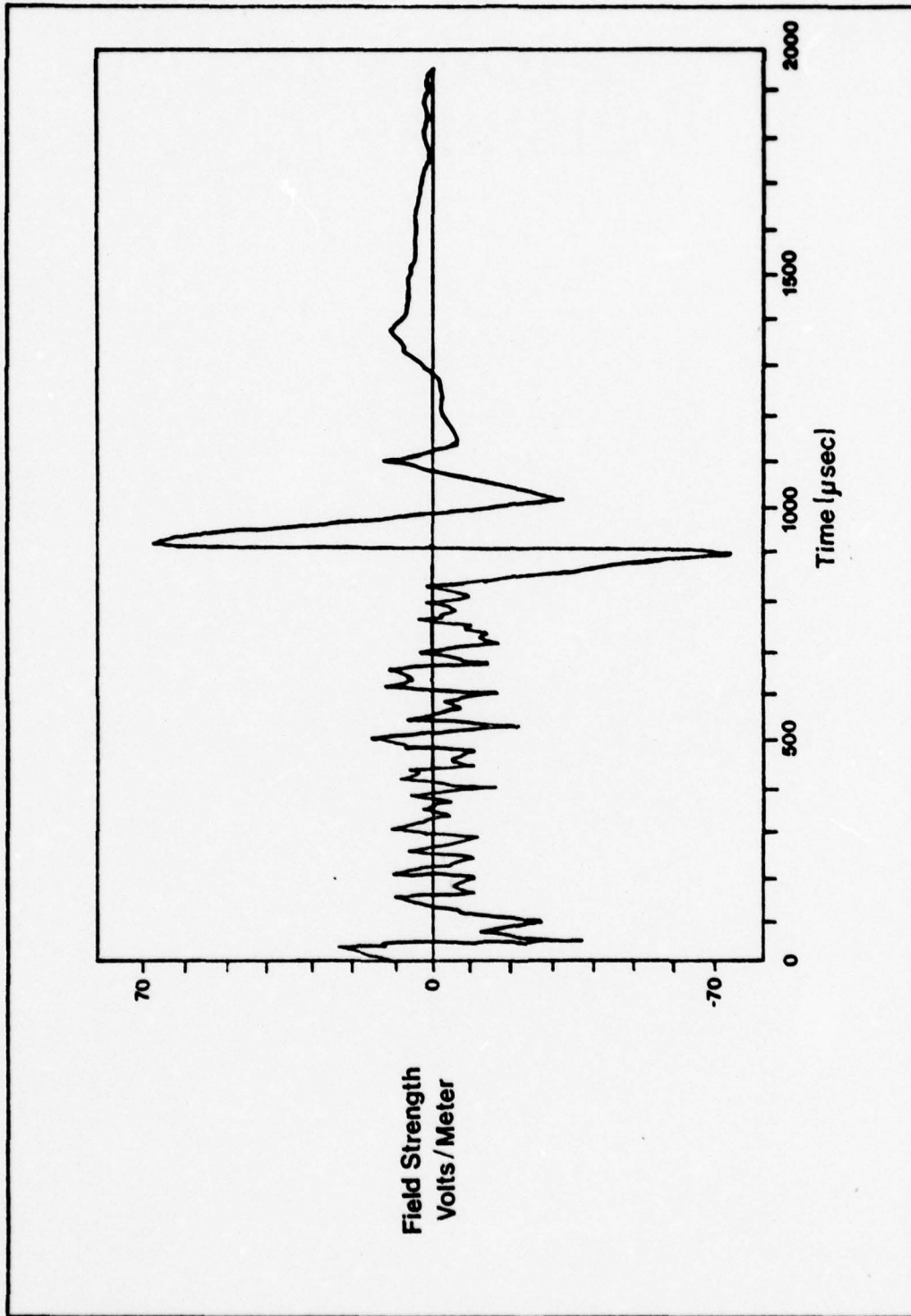


Figure 3. Measured Electric Field from a Lightning Discharge at 20 Km

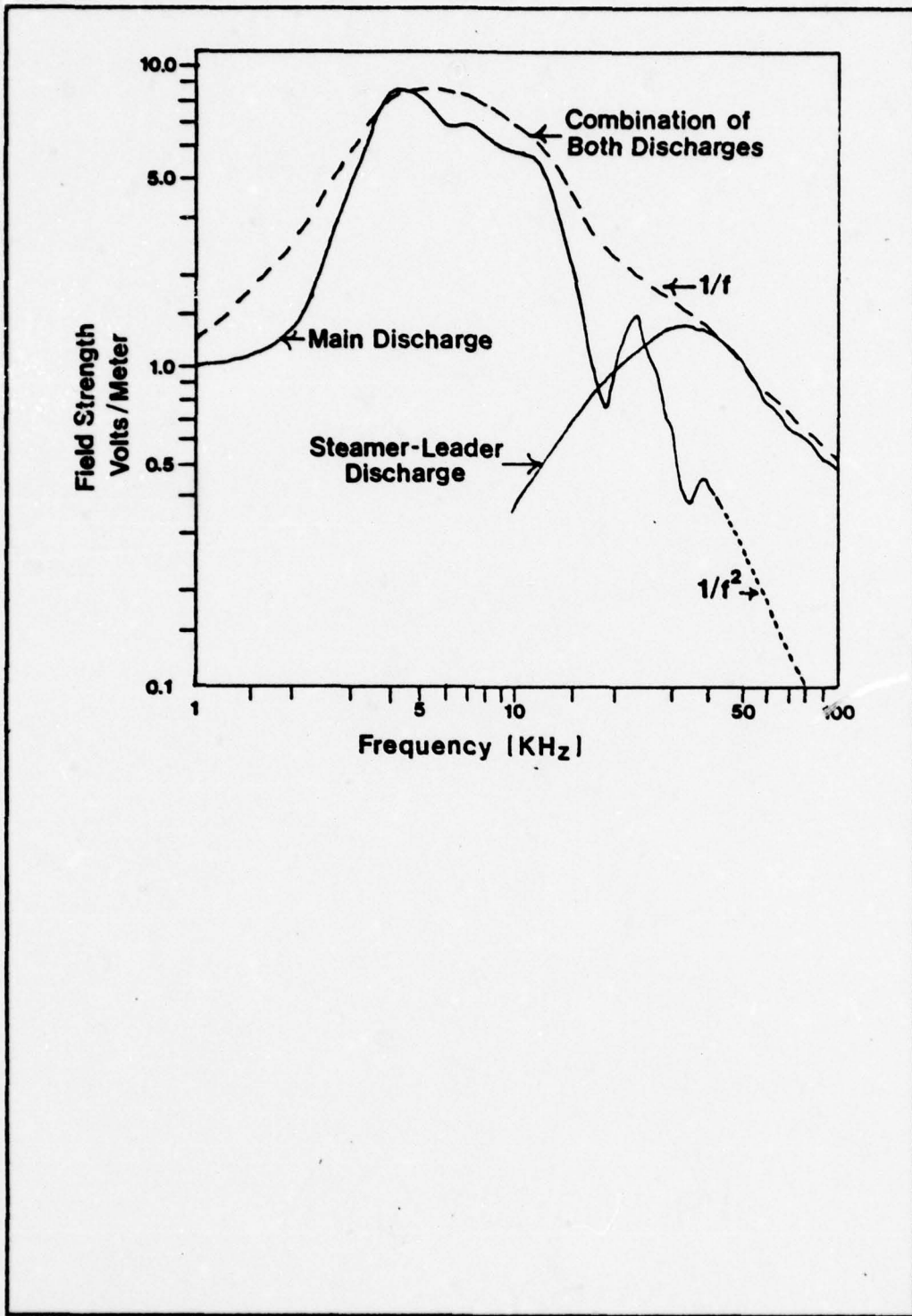


Figure 4. Measured Power Spectrum of Lightning Discharges

there are three general areas of thunderstorm activity:
South and Central America, Africa, and Indonesia.

The location of thunderstorm activity is also dependent on the time of day and the season of the year. Thunderstorm activity seems to reach a maximum in late afternoon and early evening. There is also a tendency for storm activity to follow the sun around the earth. This is demonstrated by the northward movements of storm activity in April to September, and the southward movement of the storms in October to March (Ref 31:468).

ARN is not only dependent on the location of the thunderstorms, but also the number of storms and the number of lightning discharges in those storms. The average number of thunderstorms per day has been estimated to be 44,000, or about 1800 per hour. A typical thunderstorm will produce approximately 200 discharges per hour, thus producing a total world-wide lightning discharge rate of 100 per second (Ref 4).

The propagation mechanism of the electromagnetic interference also affects the ARN at the receiver. At VLF two modes of propagation exist: ground wave and waveguide. For distances less than 1500 Km the method of propagation is essentially by ground wave. This method results in attenuation that is proportional to the distance. For distances greater than 1500 Km, but less than 20,000 Km, the earth and ionosphere act as a waveguide. The relation between the field intensity and distance, for the waveguide mode of

propagation, is given by Eq (1) (Ref 11:33).

$$E_1 = E_2 \cdot \frac{\text{EXP}(-\alpha_w d)}{d} \quad (1)$$

where

the propagation path is from point two to point one

E_i = field intensity at point i

α_w = attenuation along path w , α_w is complex with units of nepers/meter

d = distance in meters along path w

When creating a model for the ARN process it is important to understand not only the mechanisms that produce ARN, but also the effects an observation scheme might have on the noise measurements. Some of the factors affecting the measurements of ARN are receiver impulse response, antenna gain, antenna polarization, antenna directivity, and geographical location. All of these have an effect on noise measurements. These are important because noise measurements, the output of a receiver, are often used to infer the characteristics of the noise, the input to the receiver.

Statistical Characteristics of ARN

ARN cannot be described as a deterministic function of time due to the complexity of the physical processes involved. Therefore ARN is often viewed as a random process that is a function of time. This chapter investigates the known statistical properties of ARN.

A large quantity of ARN data has been gathered by the National Bureau of Standards. This data includes world-wide time averaged noise power measurements, and amplitude probability distribution curves for the time varying noise envelope. This work is presented in condensed form in CCIR Report 322 (Ref 7). The block diagram of the receiver used in these measurements is presented in Figure 5.

The world-wide measurements of ARN power are derived from measurements made by sixteen receiving stations throughout the world. Figure 6 shows the location of these stations. The average noise power available at the antenna is relatively constant for observation intervals up to four hours. The measurements made during these four hour periods are relatively constant from day to day for periods up to three months. Therefore, the noise power measurements in CCIR Report 322 are plotted for the four seasons of the year, and each seasonal section contains six plots of the four hour time blocks in a day (Ref 7). Figure 7 shows a typical average noise power plot from CCIR Report 322. The average noise figure, F_a , shown in Figure 7 is computed from Eq (2).

$$F_a = 10 \text{ LOG}_{10} \left[\frac{\left(\frac{1}{T} \int_0^T E^2(t) dt \right)}{2\pi K T_o B} \right] \quad (2)$$

where

F_a = the average noise figure in db

K = Boltzman's constant

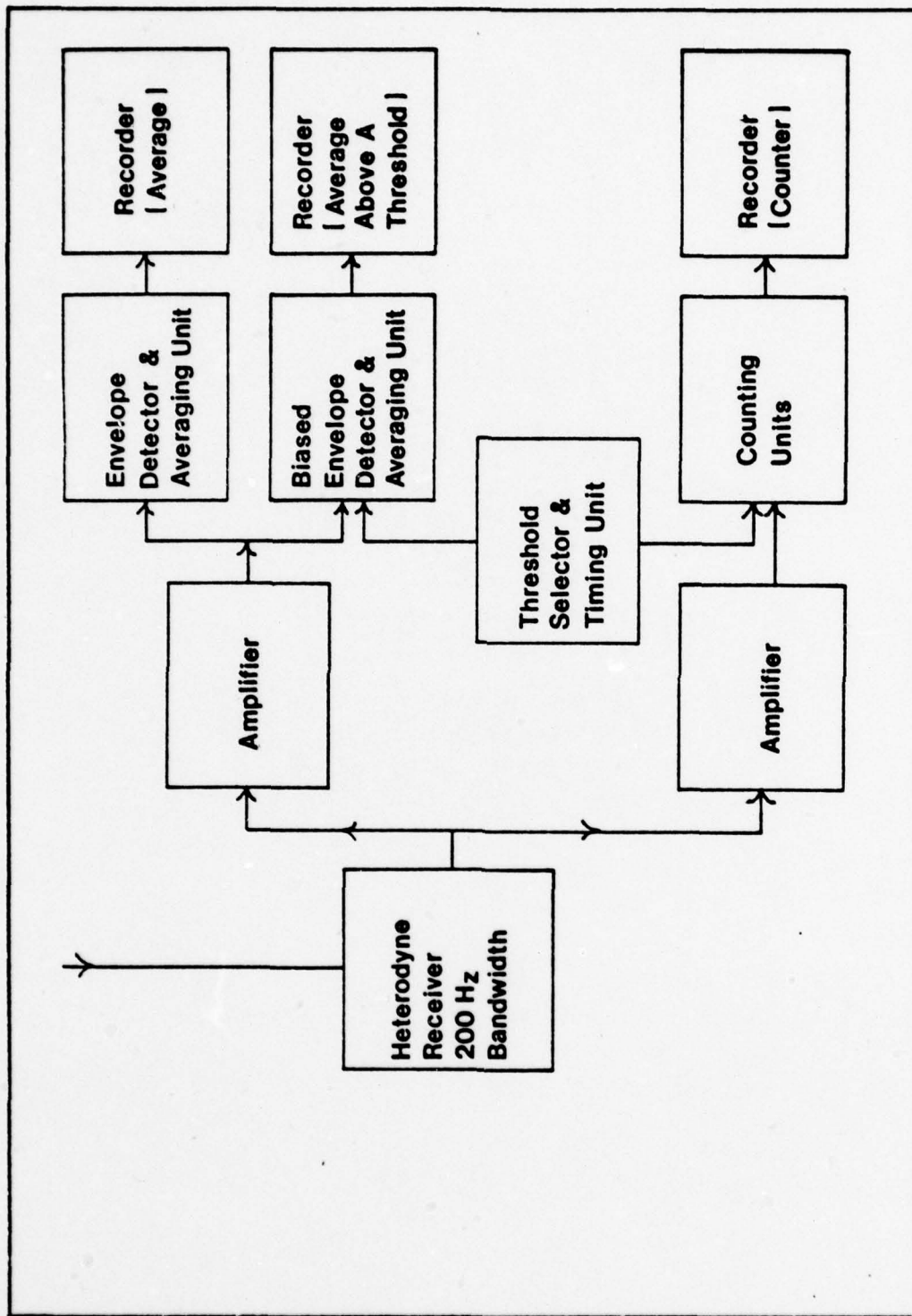


Figure 5. Block Diagram of Receiver for Measuring ARN

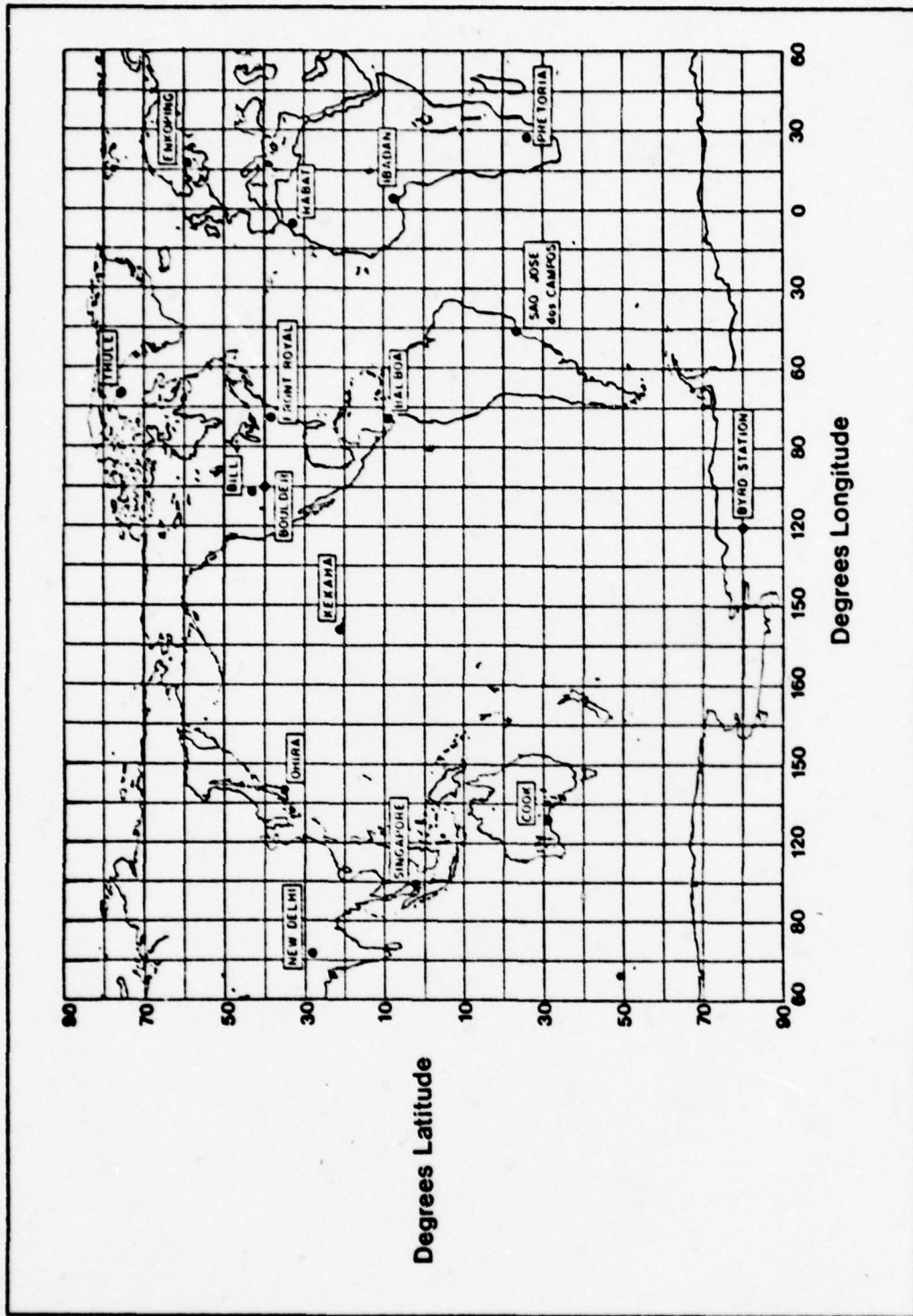


Figure 6. Location of Receiving Stations Used to Compile Data for CCIR Report 322

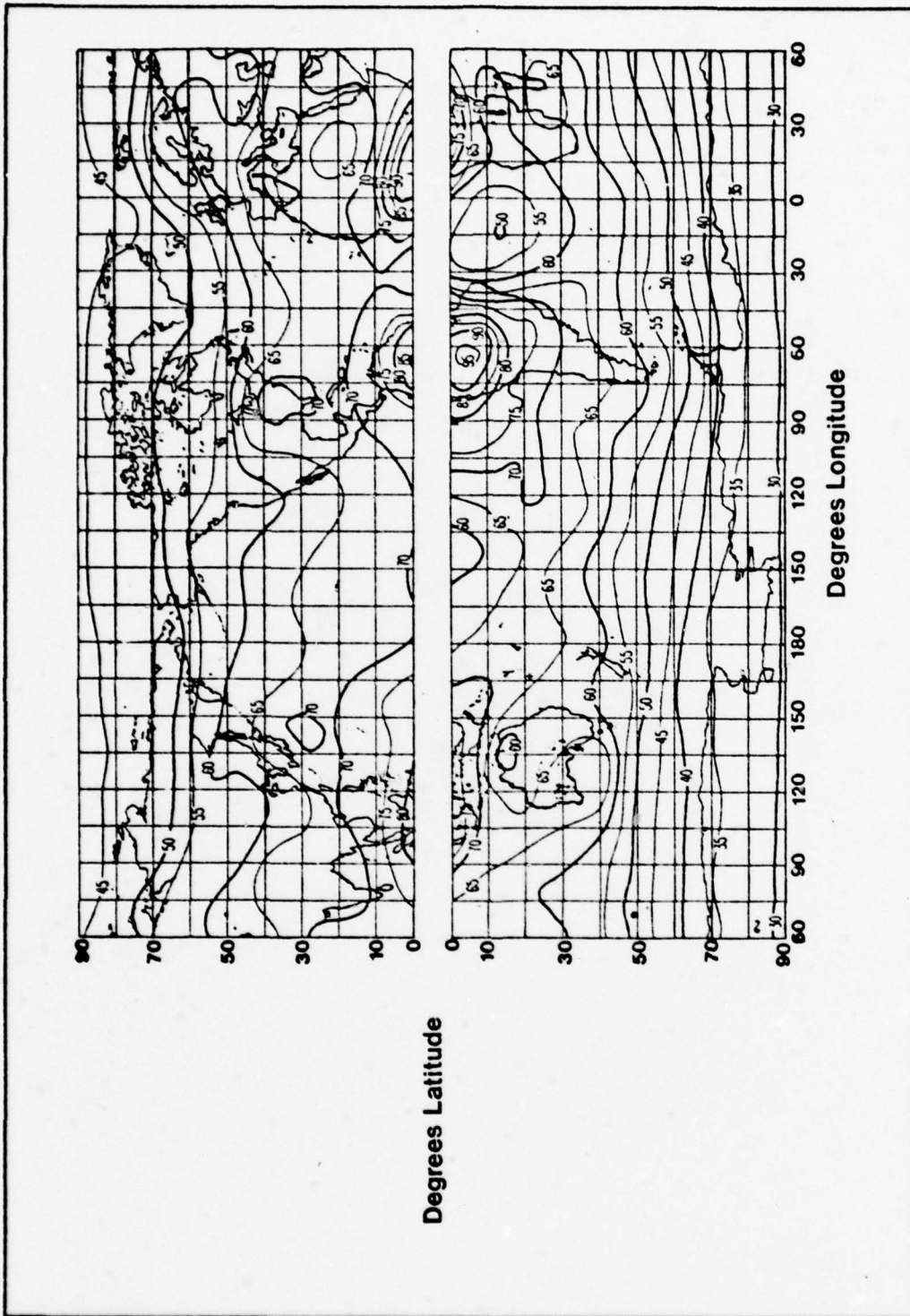


Figure 7. A Typical Plot of World-Wide Average Noise Power as in CCIR Report 322

T_o = standard temperature of 288° Kelvin

$E(t)$ = the time varying envelope waveform

T = the observation time in sec

B = the receiver bandwidth in Hertz

All of the noise power measurements in CCIR Report 322 are made by receivers with a 200 Hz effective bandwidth. Figure 8 shows an example of an empirically derived plot for converting the noise power measured at 1 MHz to the average noise power at a different frequency. A different noise power conversion plot is required for each world-wide plot of noise power.

CCIR Report 322 also contains a plot of the amplitude-probability distribution (APD) of the ARN. The APD curve is a plot showing the percentage of time that the time varying envelope voltage, at the output of an envelope detector, exceeds some threshold. The curve is plotted parametrically with V_d , which is defined by Eqs (3), (4), and (5). The V_d ratio is a rough measure of the impulsiveness of the noise; the more impulsive, the larger the V_d ratio.

$$E_{rms} = \left(\frac{1}{T} \int_0^T E^2(t) dt \right)^{\frac{1}{2}} \quad (3)$$

$$E_{av} = \left(\frac{1}{T} \int_0^T E(t) dt \right) \quad (4)$$

$$V_d = 20 \text{ LOG}_{10} \left(\frac{E_{rms}}{E_{av}} \right) \quad (5)$$

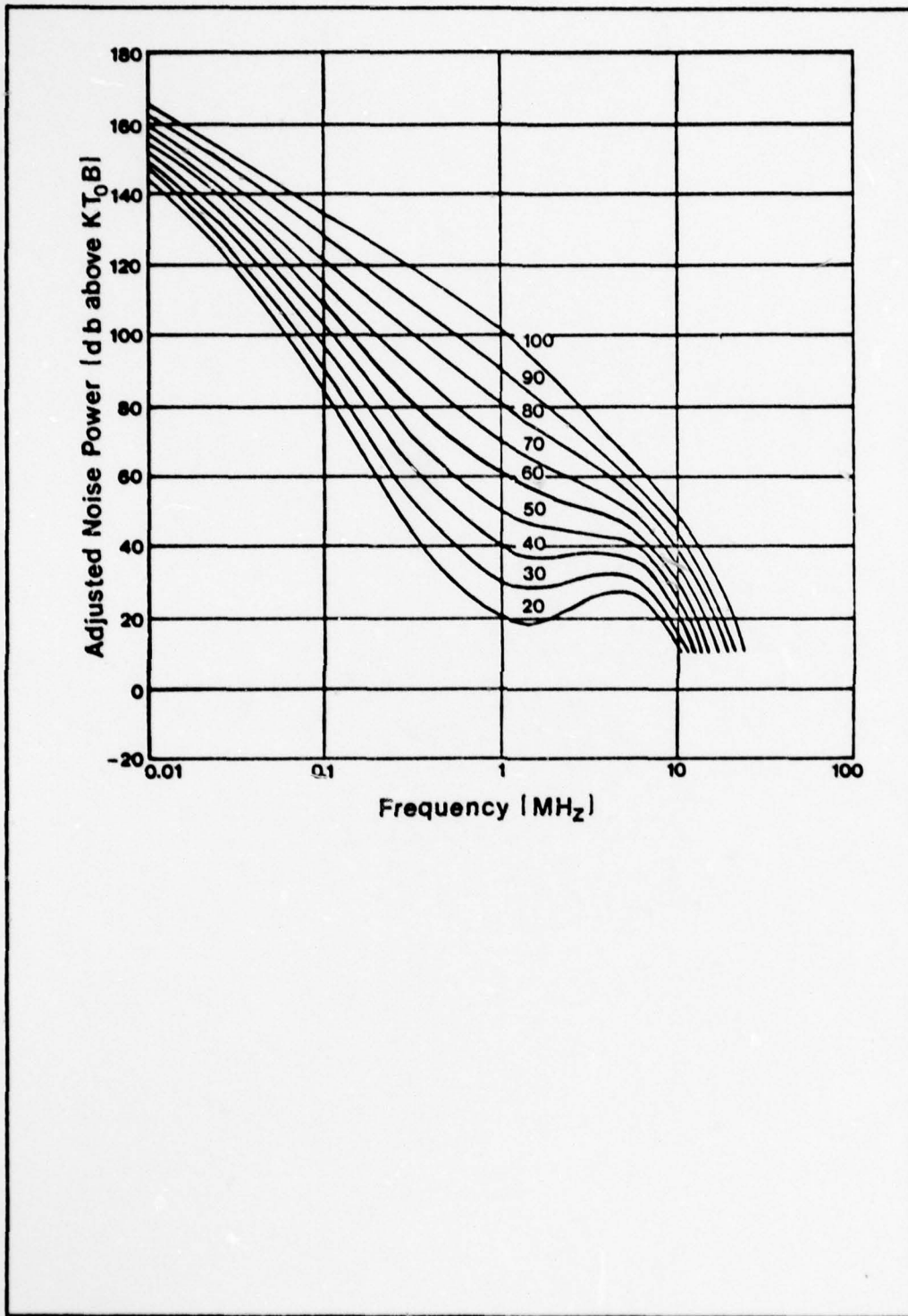


Figure 8. A Typical Noise Power Conversion Plot as in CCIR Report 322

The shapes of the APD curves depend only on the V_d ratio, rather than the absolute value of E_{rms} or E_{av} (Ref 5:1). Thus, all of the APD curves with a given V_d ratio can be collapsed into a single curve by normalizing the incoming waveform by E_{rms} , such that the resulting waveforms all have power equal to 1 watt (Ref 7:8-9). Since the waveforms have been normalized by E_{rms} , the envelope voltage threshold E_T must also be normalized. Therefore the ordinate of the APD plots is presented in terms of a threshold, Δ , which is defined in Eq (6).

$$\Delta = 20 \text{ LOG}_{10} \left[\frac{E_T}{E_{rms}} \right] \quad (6)$$

where

E_T = envelope voltage threshold

The APD plot shown in Figure 9 represents the amount of time the envelope waveform exceeds a threshold for a given V_d .

Both the noise figure, F_a , and the APD curves are dependent on the receiver bandwidth (Ref 27). The receiver used by the National Bureau of Standards has an effective noise power bandwidth of 200 Hz. The APD curves in Figure 9 can be modified to apply to receivers of bandwidth other than 200 Hz. This can be done by selecting a curve with a different V_d . Figures 10 and 11 can be used to convert a V_d ratio measured by a receiver of one bandwidth to that of a different bandwidth (Ref 27).

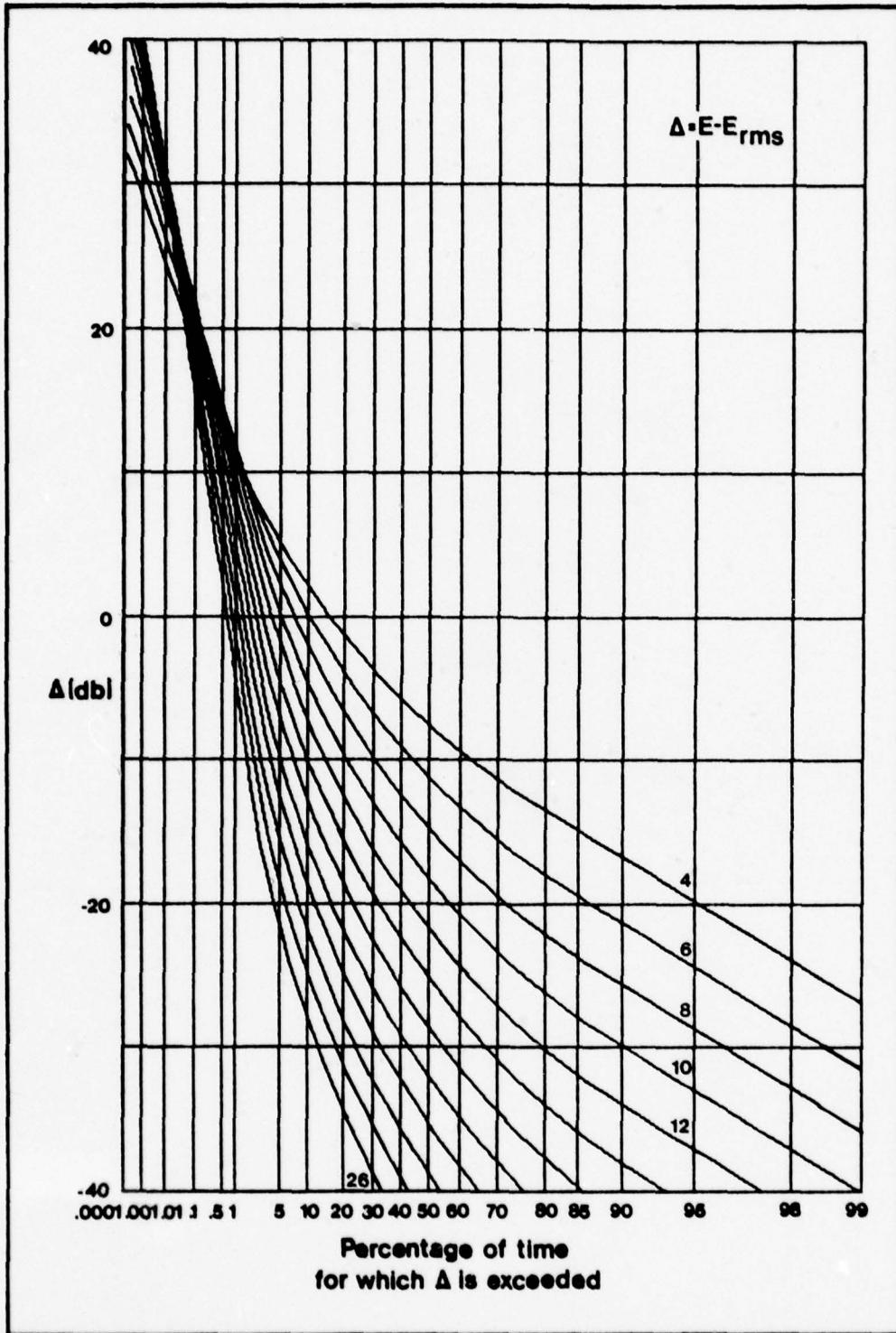


Figure 9. Measured-Probability Distribution for ARN

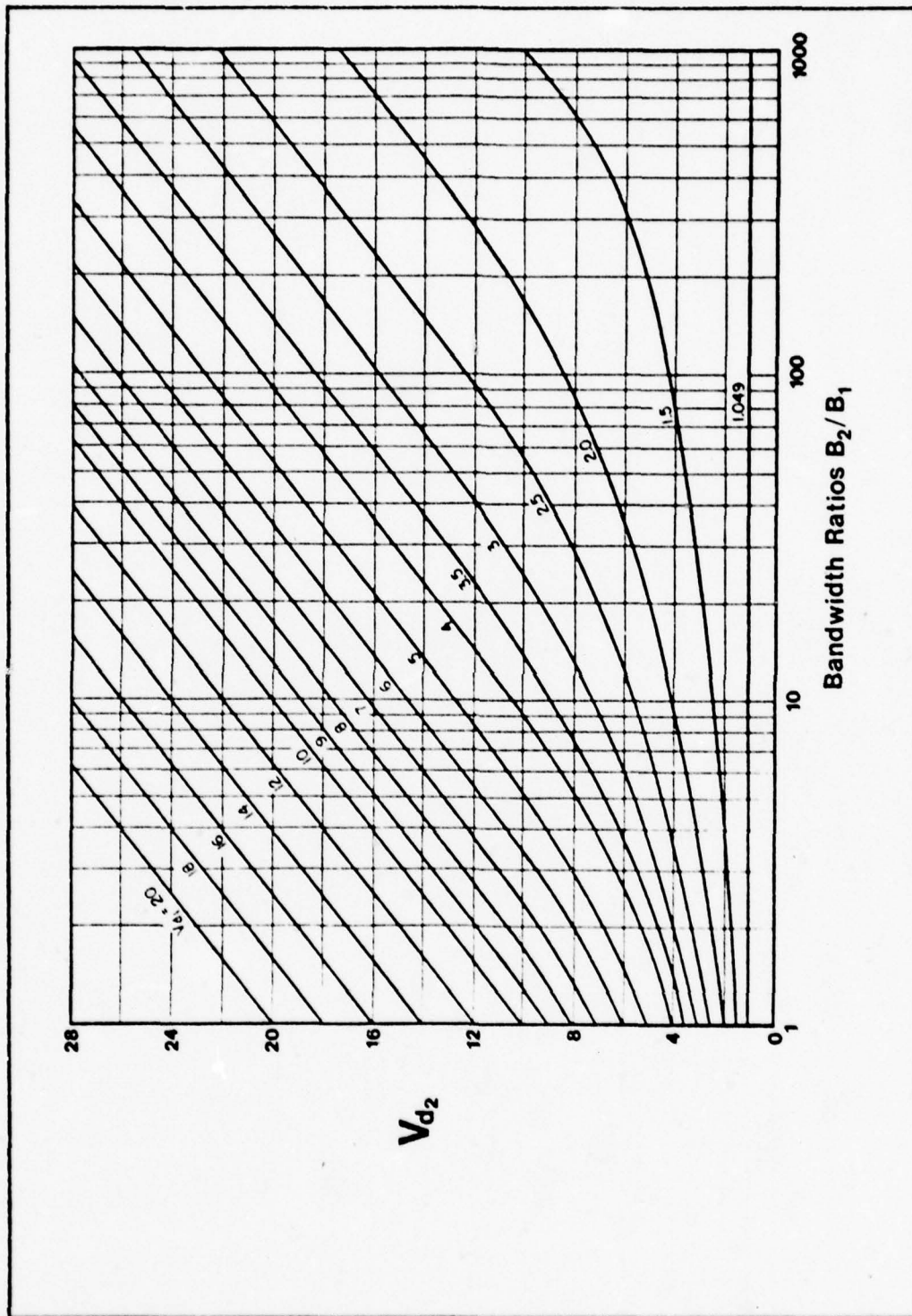


Figure 10. APD Bandwidth Conversion Plot 1

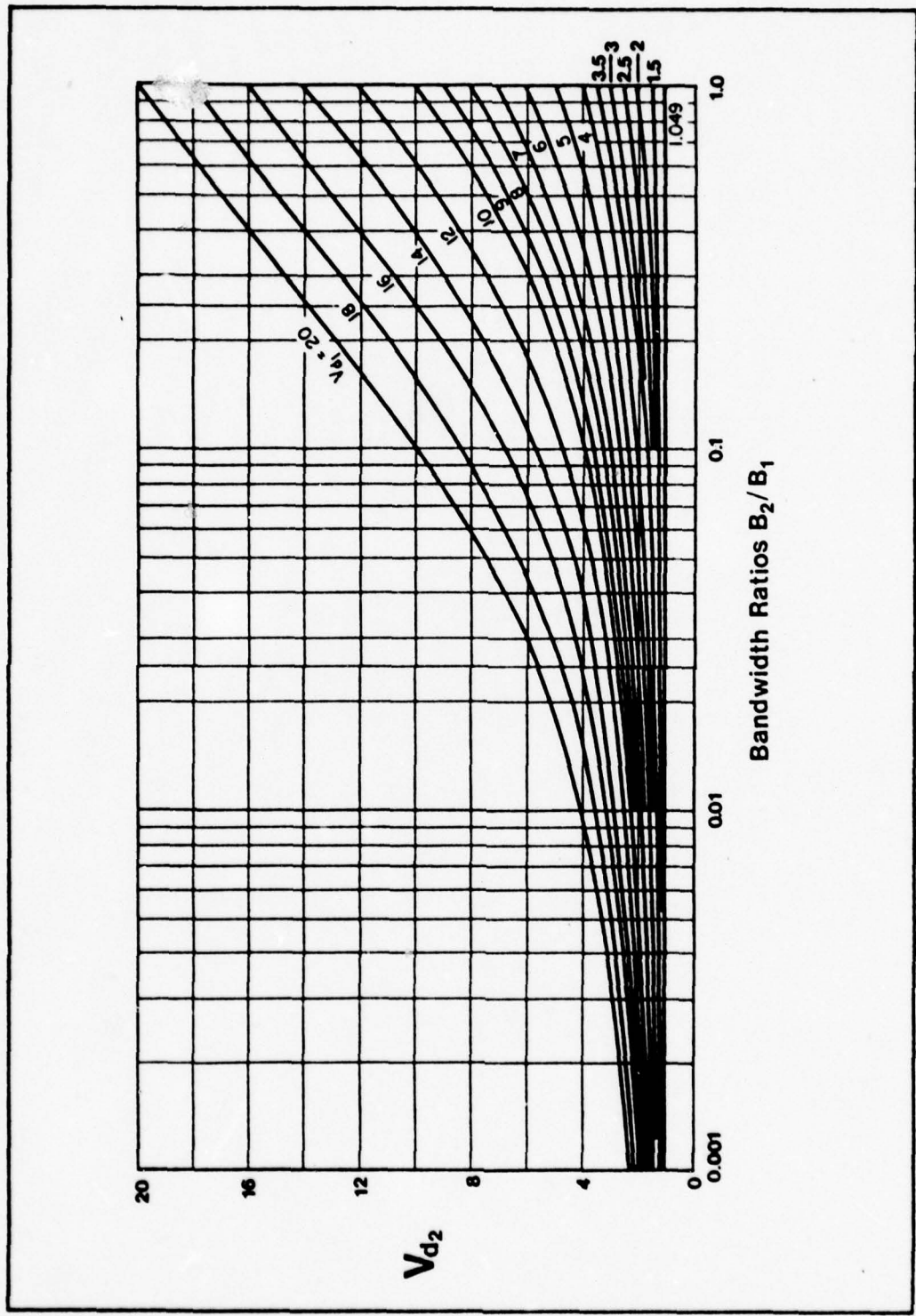


Figure 11. APD Bandwidth Conversion Plot 2

The APD curves in CCIR Report 322 are composed from measurements made in different seasons of the year and times of the day. Due to the long term variations that occur with time, the curves can only be considered an approximation to an APD curve that might be measured over any short period of time. Crichlow does not believe this introduces an appreciable error in computations using the APD curves (Ref 5:10).

All of the measurements made in CCIR Report 322 relate to the statistics of the time varying envelope waveform of the noise. If the envelope noise process is modeled as a stochastic process that is ergodic in both the mean, and autocorrelation, then the measurements of average noise power and the average envelope amplitude from CCIR Report 322 are representative of the second and first moments of the first order probability density function of the noise process. If the process is ergodic in the mean, then it is also ergodic in distribution (Ref 21:328-332). Therefore, the measured APD curves can be related to the first order cumulative distribution function of the envelope noise process. The assumption of ergodicity over at least four hour periods of time is required to make the noise measurements from CCIR Report 322 a meaningful measure of the statistical properties of the random process.

Even though a great amount of effort has been expended in making the measurements of CCIR Report 322, these measurements are at best representative of the first order statistics of the envelope noise process. When postulating a

stochastic model for ARN, the model should be based on the physical mechanisms which cause the noise. The model should also be able to represent the measured statistics. In section III this philosophy will be used to examine empirical models for ARN.

III. Empirical Noise Models

Most receivers that operate at VLF have been optimized for use in Gaussian noise, but the APD curves shown in Figure 9 demonstrate that ARN is not Gaussian. When zero-mean white Gaussian noise is the input to an envelope detector, the amplitude of the noise at the output is Rayleigh distributed. An APD curve for a Rayleigh distributed random variable plots as a straight line with a slope of negative one-half when plotted on Rayleigh paper, as in Figure 9. This corresponds to a V_d ratio of approximately 1.0, but atmospheric radio noise at VLF, usually has a V_d ratio between 4 and 14. Thus, Gaussian noise is not a good approximation of ARN.

Philosophy of Empirical Models

When evaluating the performance of VLF receivers, an analytically tractable model for ARN must be used. One approach, that has been used many times, is to find a random variable that has a first order density function that will produce an APD curve that matches the measured curves shown in Figure 9.

This type of model has been used to evaluate the performance of communication systems operating in ARN (Refs 10; 19;21;24;32). Models of this type are referred to as empirical models (Refs 11;12).

There are two requirements that all useful empirical models must meet. First, the model must be capable of producing theoretical APD curves that match measured curves. Second, the model must be analytically tractable. Both of these requirements are somewhat vague since the first does not specify how precisely the model must match the measured data, and the second does not specify how tractable a model must be for a given application.

An upper limit on the required accuracy of fit can be established by determining the variation in the measured data that produced the APD curves in CCIR Report 322. The APD curves shown in Figure 12 are composed from data obtained over short periods of time (short term APD curves). All of these curves have the same V_d ratio, but differ slightly in shape. The APD curves in CCIR Report 322 (long term APD curves) are the result of combining all the data used to produce the short term APD curves of a given V_d ratio. In a later chapter, long and short term APD curves are compared using a quantitative measure of the quality of fit between curves. Since nothing is gained by making theoretical curves fit measured curves closer than the accuracy of measured data, the fit between short and long term APD curves is used as an upper limit of accuracy when fitting APD curves.

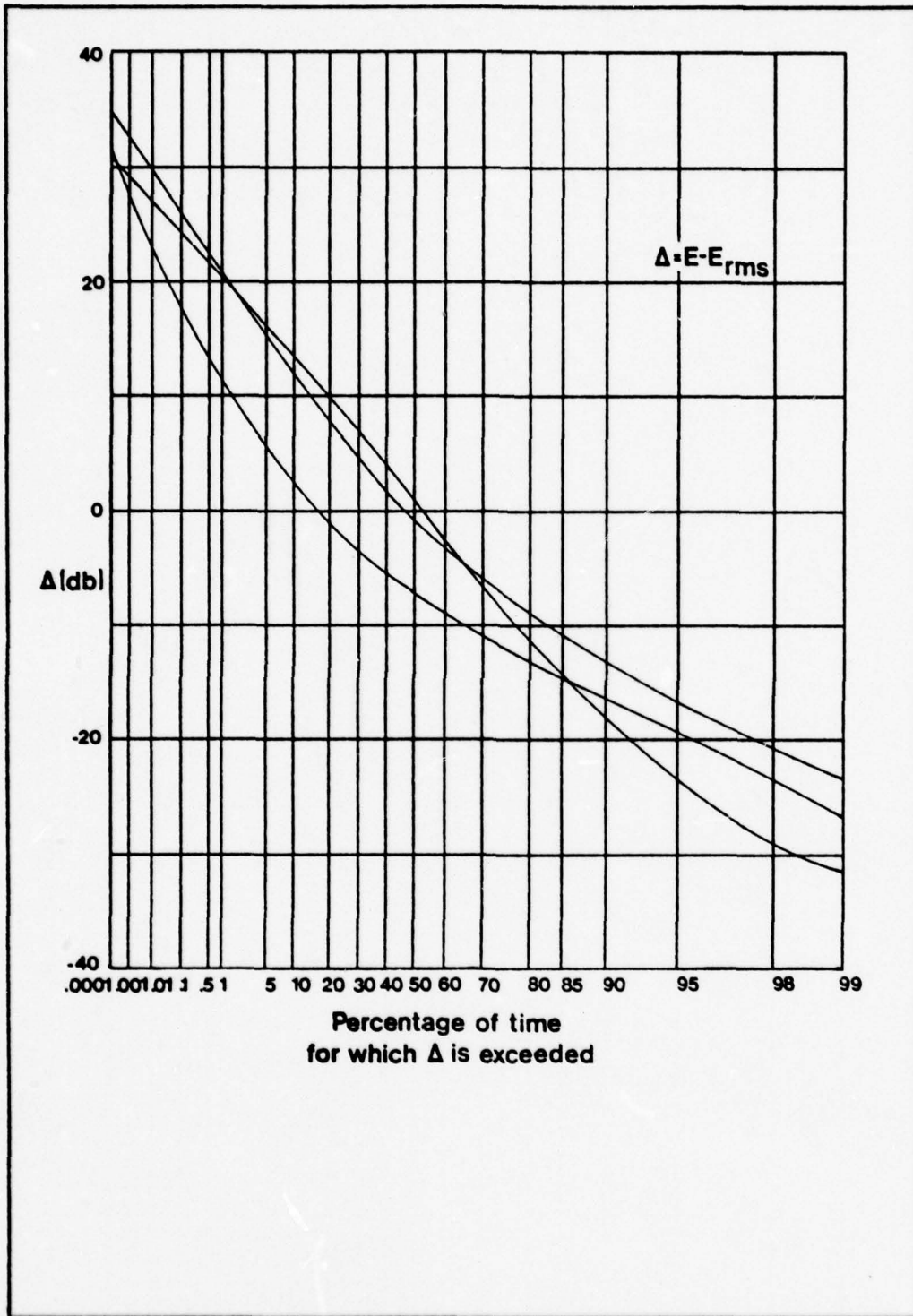


Figure 12. Short Term APD Curves, $V_d = 4$

Survey of Empirical Models

This section presents a survey of empirical models. The models are discussed in terms of the following characteristics: formulation, assumptions, strengths and weaknesses.

APD Representation by Crichlow (Refs 5;6;7). Crichlow's representation of the APD curves is based only on measured data. Crichlow observed, when APD data is plotted on Rayleigh probability paper, as in Figure 9, the plots consist of two straight line segments of different slopes connected by a curved section. The grid coordinates for Rayleigh probability paper are defined in Eqs (7) and (8).

$$X = - \frac{1}{2} \text{LOG}_{10} \left\{ - \text{LN} [P(E)] \right\} \quad (7)$$

$$Y = 20 \text{LOG}_{10} \left[\frac{E}{E_{\text{rms}}} \right] \quad (8)$$

where

X is abscissa scale in linear units

Y is ordinate scale in linear units

P(E) is the probability that the envelope exceeds a threshold, E

E is envelope threshold voltage

E_{rms} is RMS value of the time varying envelope waveform

The three sections of the APD curves can be analytically represented by three separate functions. When combined the functions form a piecewise continuous approximation to the APD curves. The three functions can be piecewise

differentiated to produce a first order density function of the noise envelope. This process is used by Wilson (Ref 32:27-48).

The main advantage of the Crichlow representation is its accuracy in reproducing measured APD curves. The disadvantages of this representation are (1) the model is not based on the physical mechanism that causes the noise, (2) the model gives no information about higher order statistics of the noise, and (3) no convenient method exists to relate the V_d ratio of the noise to parameters of the model.

Beckman's Lognormal APD Model (Ref 3). Beckman's model is based on some assumed underlying mechanism that cause ARN. Beckman assumes the observed ARN envelope results from an appropriate transformation of two statistically independent noise vectors. The first is Rayleigh distributed in amplitude and is assumed to have uniform phase; the second is lognormally distributed in amplitude and is assumed to have uniform phase. The Rayleigh vector represents continuous background noise from distant storm activity. The lognormal vector results from the propagation mechanism affecting highly impulsive noise from nearby thunderstorm activity. Appendix A presents some properties of the Beckman model. Eq (9) expresses the first order density function of the noise envelope, seen at the output of the receiver shown in Figure 5.

$$f(\underline{E}) = \frac{2}{Nc\sigma\sqrt{2\pi}} \int_0^{\infty} \frac{E}{E_0} \left[\text{EXP} \left(- \frac{E^2 + E_0^2}{Nc} - \frac{(\text{LN}(E_0) + \sigma^2)^2}{2\sigma^2} \right) \right] I_0 \left(\frac{2EE_0}{Nc} \right) dE_0 \quad (9)$$

where

\underline{E} is the random envelope amplitude at the output of the envelope detector

Nc is a variable between 0 and 1 that depends on the number of lightning discharges and the receiver bandwidth

σ^2 is the variance of the lognormal variable

$I_0(\cdot)$ is the zero order modified Bessel function

The advantages of Beckman's model are (1) its accuracy in representing measured APD curves, and (2) its basis on physical mechanisms causing ARN. The disadvantages of Beckman's model are (1) the density function cannot be expressed in closed form, (2) the parameters of the model must be determined by trial and error, (3) the V_d ratio for this model cannot be expressed in closed form, and (4) the model cannot be extended to higher order statistics. Thus, Beckman's model is representative of the measured data, but is very difficult to use in practical applications.

Beach and George Noise Model (Ref 2). The Beach and George model is similar to Beckman's model except that an attempt is made to account for the dependence between large noise pulses caused by multiple lightning discharges from

nearby storm activity. The model produces good agreement with measured APD curves for low probability of exceedence, but produces poor agreement at high probability of exceedence. This model has many of the analytical problems of Beckman's model and results in a poor fit to the measured APD curves. Therefore, the model by Beach and George is not recommended for modeling ARN.

Hall's Generalized t Model (Refs 12;24). Hall's model assumes the observed noise at the input of the envelope detector can be represented by the product of two random processes; the first process is narrow band zero-mean Gaussian noise, $N(t)$, and the second process is a slowly varying amplitude modulated process, $A(t)$. $A(t)$ is a stationary process with a first order density function given by the two-sided Chi distribution as defined by Papoulis (Ref 21:250). It is assumed the two processes are statistically independent. The two processes are multiplied together to produce a random process representation of the noise at the input of the envelope detector receiver shown in Figure 5.

This model has only one advantage, APD and density functions can be expressed in closed form. The disadvantages are (1) parameters of the model are not related to any characteristics of the actual noise, (2) the model is only capable of matching APD curves over a small range of V_d ratios, and (3) the resulting APD curves do not match

measured curves for extreme values of threshold. Even though the model may be used to find higher order statistics of the noise process at the input of the envelope detector, it is not clear that these statistics represent the higher statistics of the actual noise, since the model is not based on the physical mechanisms causing the noise. Thus, Hall's model is also a poor representation for ARN.

M-Distribution Model (Ref 18). The M-distribution model describes atmospheric radio noise at high frequency. This model cannot be extended to VLF because of the limited range of V_d ratios produced by this model. Therefore use of the M-distribution model must be limited to medium and high frequencies.

Power Rayleigh Model for ARN (Ref 8:83-87). The power Rayleigh model is similar to the Beckman model. The power Rayleigh model is composed of an appropriate transformation of two independent noise vectors at the output of the envelope detector. The first vector is Rayleigh distributed in amplitude and uniformly distributed in phase, the second is power Rayleigh distributed in amplitude and uniformly distributed in phase. Eq (10) is the first order density function of a power Rayleigh random variable, while Eq (11) shows the first order density resulting from the sum of the Rayleigh and power Rayleigh random variable.

$$f(y) = \frac{\alpha y^{\alpha-1}}{R^\alpha} \text{EXP}\left[-\left(\frac{y}{R}\right)^\alpha\right] \quad (10)$$

$$f(z) = 2 \int_0^\infty \frac{\alpha y^{\alpha-1}}{R^\alpha} \text{EXP}\left[-\left(\frac{y}{R}\right)^\alpha\right] \cdot \frac{z-y}{R_0^2} \text{EXP}\left[-\left(\frac{z-y}{R_0}\right)^2\right] dy \quad (11)$$

where

$$0 \leq \alpha \leq 2$$

$$y \geq 0$$

z is the resulting first order density of the noise envelope

This model has many of the same advantages and disadvantages as the Beckman model. It produces APD curves that are close to measured curves, but not as close as the curves from Beckman's model. With this model the V_d ratio can be expressed in closed form, but unfortunately the exceedence probability cannot. As in Beckman's model, the parameters must be determined by trial and error.

Mixture Model (Ref 24:38-43). The mixture model is based on the probabilistic mixture of two random processes. One is an impulsive process, $S(t)$, and the other is a Rayleigh process, $Z(t)$. Both are found at the output of the envelope detector Figure 5. Eq (12) shows the total noise process, $N(t)$.

$$N(t) = \frac{S(t) + Z(t)}{2} + \frac{S(t) - Z(t)}{2} \cdot v(t) \quad (12)$$

where

$U(t) = 1$ with probability p

$U(t) = -1$ with probability $1-p$

Thus, if the random process $N(t)$ is observed, $N(t)$ equals $S(t)$ on Mp of the observations, and $N(t)$ equals $Z(t)$ on the remaining $M(1-p)$ observations, where M is the total number of observations. Both $Z(t)$ and $S(t)$ are assumed to be quasistationary with first order density function given by Eqs (13) and (14).

$$f(z) = \frac{z}{\sigma^2} \text{EXP} - \left[\frac{z^2}{2\sigma^2} \right] \quad (13)$$

$$f(s) = \frac{s^r}{(k\sigma)^{r+1} \Gamma(r) 2^{r-1}} \cdot K_{1-r} \left(\frac{s}{k\sigma} \right) \quad (14)$$

where

$$Z \geq 0$$

$$S \geq 0$$

$2\sigma^2 =$ the second moment of Z

k and r are parameters of the model

$\Gamma(r) =$ the gamma function of r

$K_{1-r}(x) =$ a modified Bessel function of order $1-r$

The exceedence probability for the mixture model is given by Eq (15).

$$P(E) = \left(\frac{E}{k\sigma} \right)^r \frac{1}{2^{r-1} \Gamma(r)} K_r \left(\frac{E}{k\sigma} \right) \cdot p + (1-p) \cdot \text{EXP} - \left[\frac{E}{2(\sigma_0)^2} \right] \quad (15)$$

Advantages of the mixture model are the first order statistics can be expressed in closed form, and the exceedance probability, given by Eq (15), produces a fairly good fit to the measured APD curves, except at extremes of the voltage thresholds. The biggest disadvantage in using the mixture model is the parameters k , r , σ , p must be determined by trial and error. As with other empirical models, it is not possible to find useful higher order statistics of the noise.

Measuring the Exactness of Fit for APD Curves

The purpose of this section is twofold. First, a quantitative measure for closeness-of-fit between measured and theoretical APD curves is developed. Second, this measure of fit is used on two different empirical models and on short-term APD curves to establish acceptable values of fit between APD curves for use in Chapter IV.

Two empirical models are examined to determine their quality in terms of fit between measured and theoretical APD curves. The measured and theoretical APD curves are compared at nine different values of threshold, Δ , the nine values of threshold being at 10 db intervals from -40 db to 40 db. Two different values of V_d are used in the comparison, V_d equal to 4 and 10; these are typical V_d ratios found at VLF. The fidelity criterion for closeness-of-fit is given by Eq (16).

$$\text{MSE} = \frac{\sum_{i=1}^9 (d_i)^2}{\sum_{i=1}^9 (P_{1i})^2} \quad (16)$$

where

d_i = the linear distance between the curves when plotted on Rayleigh probability at a given Δ_i

P_{1i} = the exceedence probability from the measured APD curve at Δ_i

This is a sample mean-square error measure where d is the linear distance on Rayleigh paper along the exceedence axis. The linear distance may be computed by Eq (17).

$$d_i = \text{LOG}_{10} \left[\frac{\text{Ln}(P_{1i})}{\text{Ln}(P_{2i})} \right] \quad (17)$$

where

Ln is the natural logarithm

P_{1i} = the exceedence probability from the measured APD curve at Δ_i

P_{2i} = the exceedence probability from the theoretical APD curve at Δ_i

d_i = linear distance between P_{1i} and P_{2i}

Figures 13, 14, 15, and 16 show the fit of the mixture model and the Beckman model to measured APD curves at V_d ratios of 4 and 10. The error statistic, MSE, for each curve is shown on the figure it applies to.

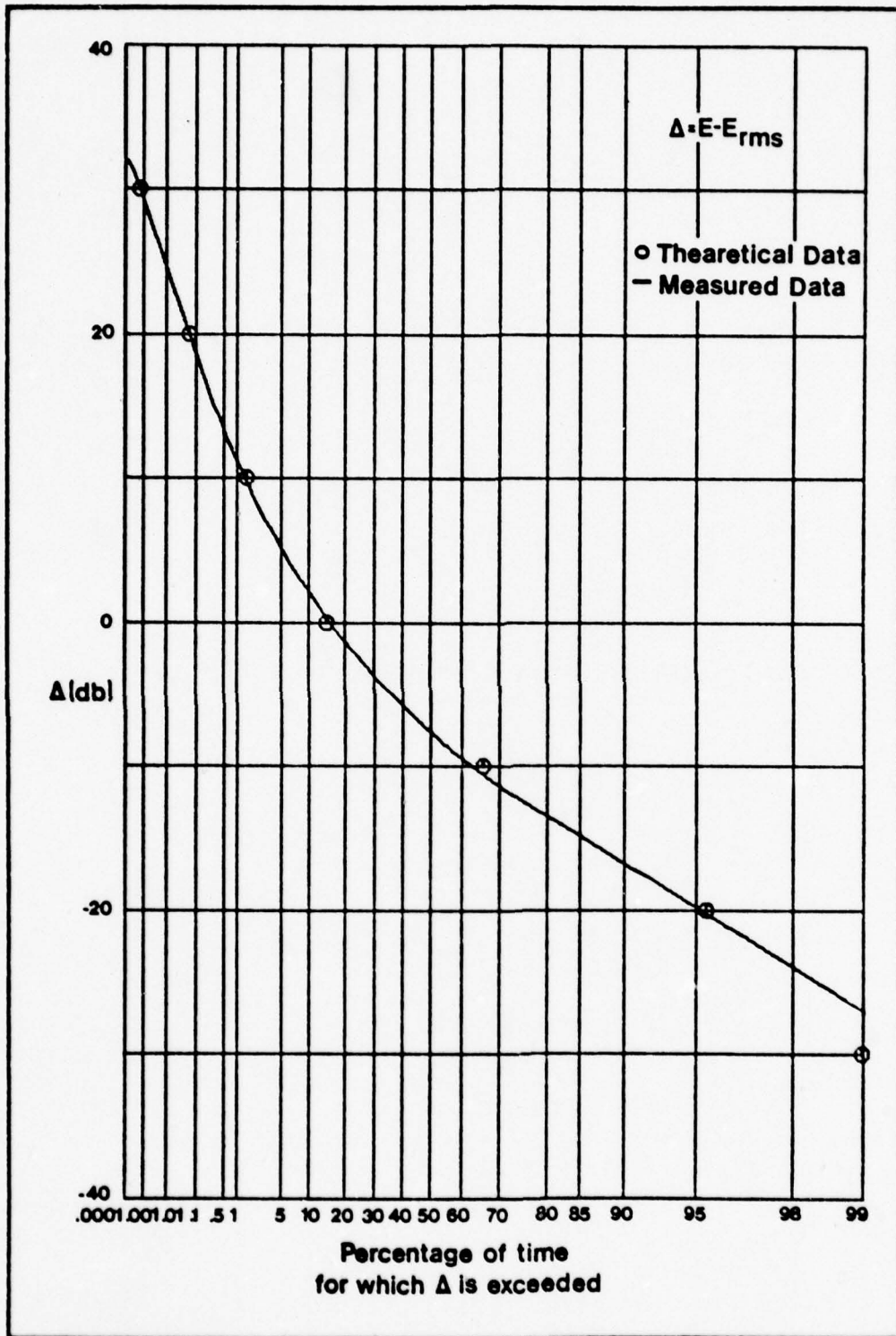


Figure 13. Comparison of Measured and Beckman APD Curves, $V_d = 4$ (MSE = .00924)

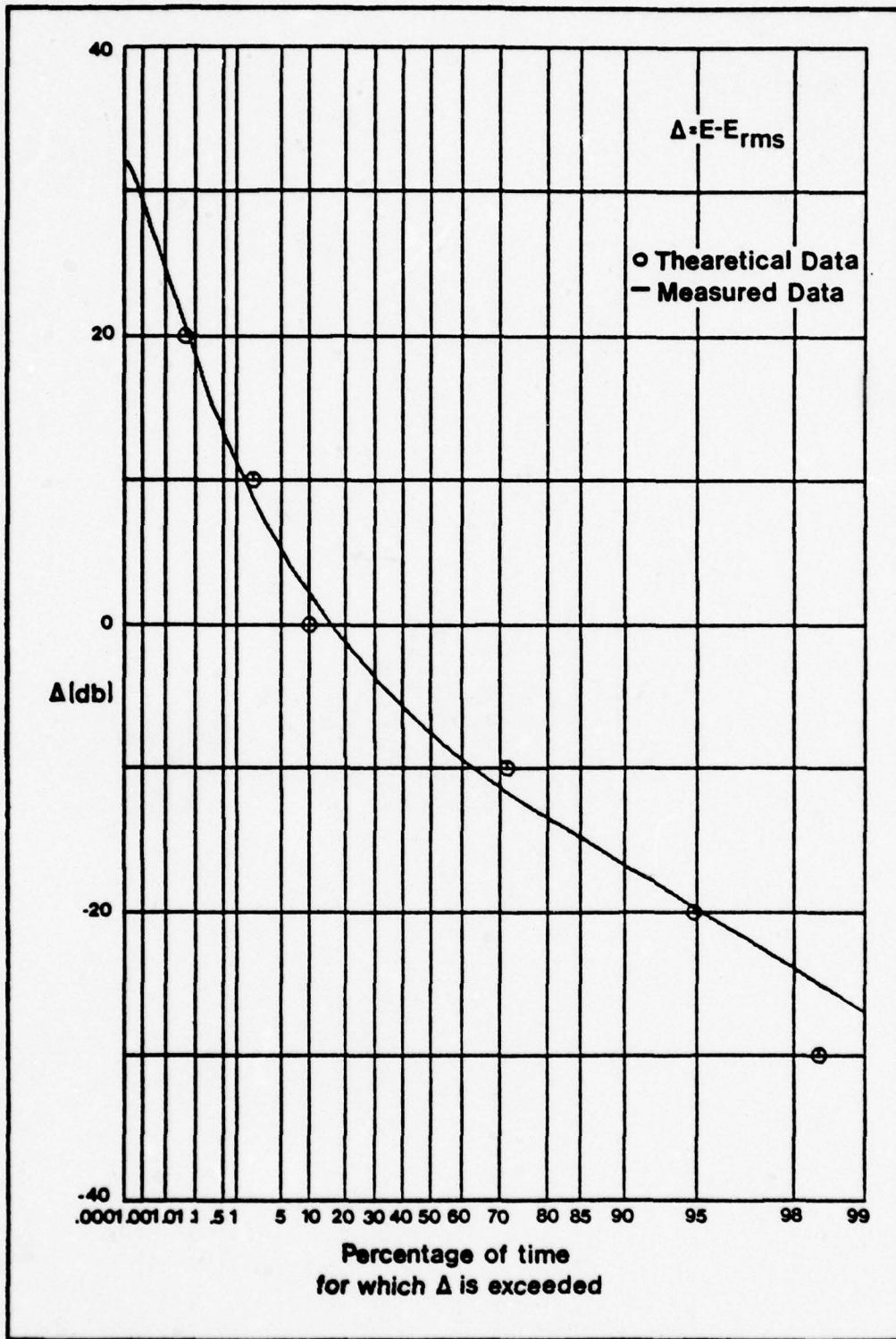


Figure 14. Comparison of Measured and Mixture APD Curves, $V_d = 4$ (MSE = .081)

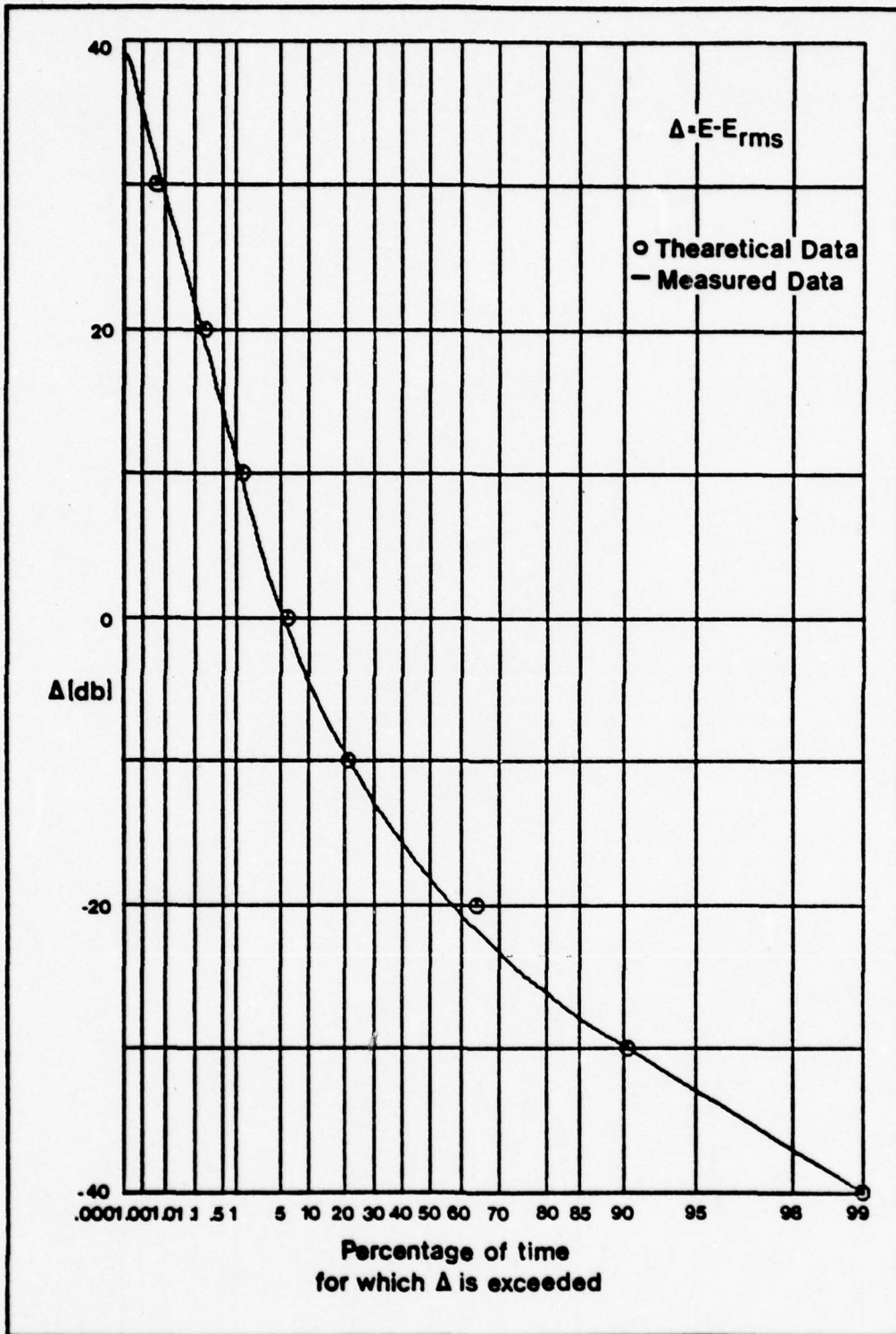


Figure 15. Comparison of Measured and Beckman APD Curves, $V_d = 10$ (MSE = .00146)

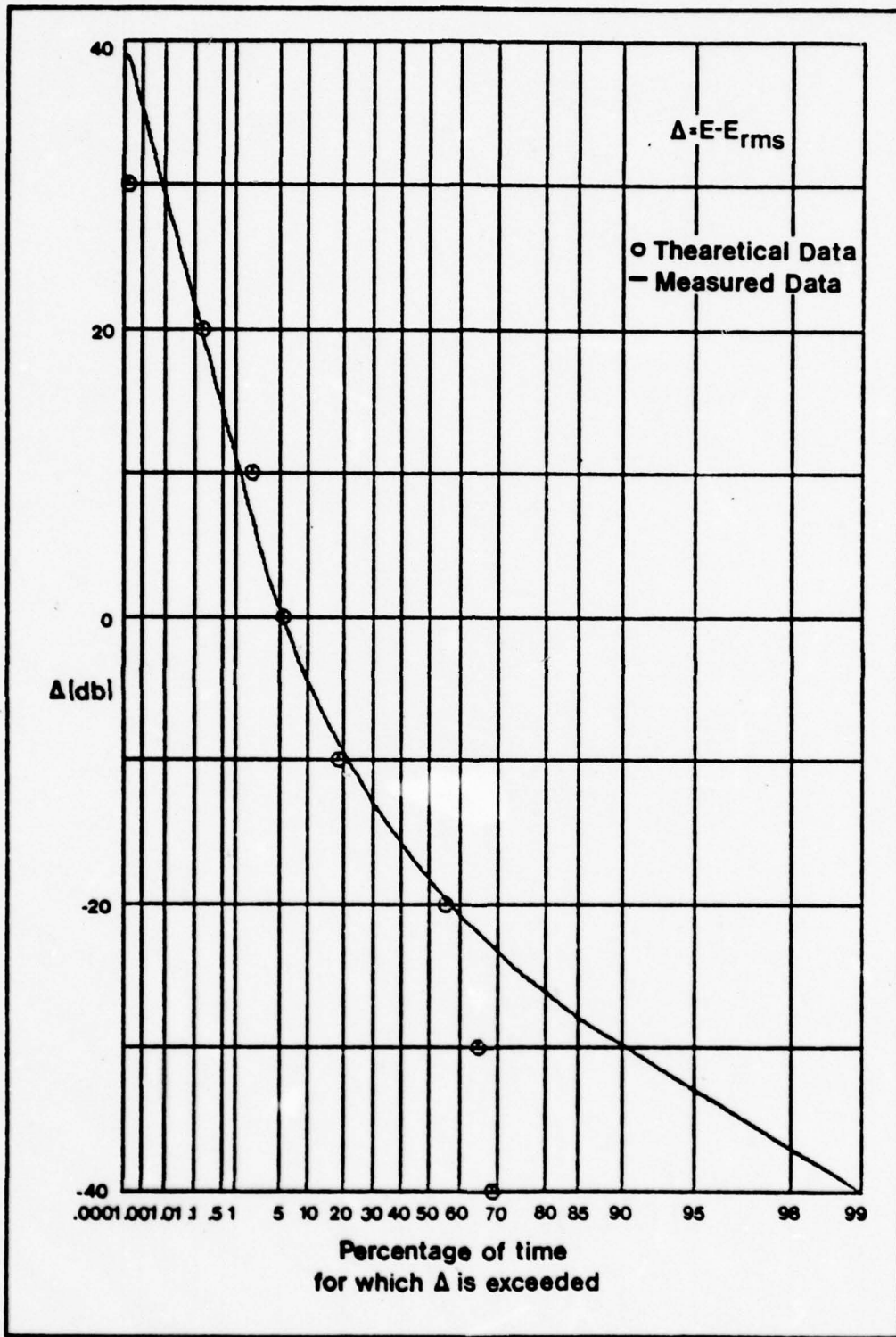


Figure 16. Comparison of Measured and Mixture APD Curves, $V_d = 10$ (MSE = .347)

The major purpose of examining these two models is to establish an acceptable measure of exactness of fit for theoretical APD curves. The Beckman model is used because it provides the closest fit to measured APD curves, and the mixture model is used because it is the most convenient empirical model. The value of MSE is shown on each plot. Nine points are used to determine the value of MSE for each curve even though all nine points do not always appear on the plot because of scaling considerations. The error between short term and long term APD curves produced MSE values ranging from .041 to .152 for V_d equal to 4, and from .027 to .086 for V_d equal to 10. This indicates both empirical models fit the measured data reasonably well.

Inherent Deficiencies of Empirical Noise Models

ARN is represented in a probabilistic manner to provide the communication engineer a method for evaluating the performance of existing receiver configurations, and to allow him to specify the optimal receiver structure. This section examines the requirements for evaluating receiver performance and specifying the optimal receiver. The adequacy of empirical noise models are examined in terms of these requirements.

Evaluating the Performance of Existing Receiver Structures. As mentioned earlier, most VLF receivers currently operational are optimal in a white Gaussian noise environment. In this section, a binary receiver, that is optimal in white Gaussian noise, is used as an example for the analysis

of a known receiver structure, see Figure 17. Before a receiver can be evaluated, a criteria must be established by which performance is measured. Minimum probability of error is the criteria used in this section (Refs 29; 24). It is assumed that both signals are equally likely, have equal energy, and are known exactly. The resulting receiver structure is examined in many textbooks; its performance is well known (Refs 29:27-28; 14:67-68; 33:248-251).

This receiver computes realizations of two random variables, \hat{x}_1 and \hat{x}_2 , over the signaling interval of length T. It then computes a new random variable realization, $\hat{\Lambda}$, by subtracting \hat{x}_2 from \hat{x}_1 . Eqs (18), (19), and (20) demonstrate the computations made by the receiver.

$$\hat{x}_1 = \int_0^T S_1(t) [S_i(t) + \underline{n}(t)] dt \quad (18)$$

$$\hat{x}_2 = \int_0^T S_2(t) [S_i(t) + \underline{n}(t)] dt \quad (19)$$

$$\hat{\Lambda} = \hat{x}_1 - \hat{x}_2 \quad (20)$$

where

$S_i(t)$ is the i th signal

$\underline{n}(t)$ is the additive noise

$\underline{r}_i(t)$ is the received signal plus noise

There are two conditional densities associated with each of the random variables, \hat{x}_1 and \hat{x}_2 . These are $f(\hat{x}_1 | S_1)$,

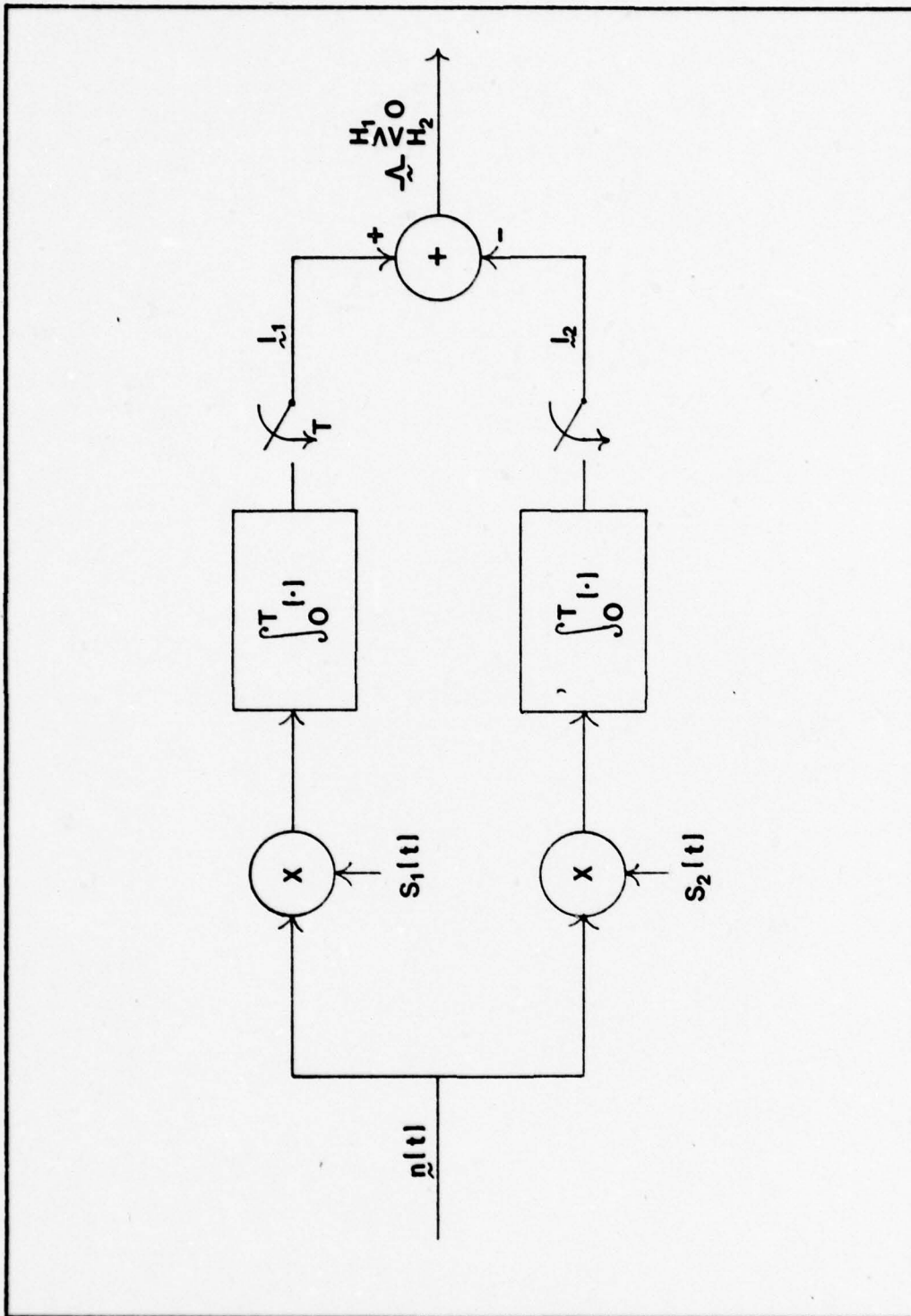


Figure 17. Optimal Binary Receiver for White Gaussian Noise. Signals are Equally Likely and Have Equal Energy

$f(\underline{\ell}_1|S_2)$, $f(\underline{\ell}_2|S_1)$, and $f(\underline{\ell}_2|S_2)$; where $f(\underline{\ell}_i|S_j)$ is the density on $\underline{\ell}_i$, assuming S_j is transmitted. Since the decision statistic $\underline{\Lambda}$ is the difference of two random variables, the conditional densities of $\underline{\Lambda}$ depends on joint densities of $\underline{\ell}_1$ and $\underline{\ell}_2$. Eqs (21) and (22) show these densities.

$$f(\underline{\Lambda}|S_1) = f(\underline{\ell}_1 - \underline{\ell}_2|S_1) \quad (21)$$

$$f(\underline{\Lambda}|S_2) = f(\underline{\ell}_1 - \underline{\ell}_2|S_2) \quad (22)$$

Since the performance of the receiver is measured in terms of probability error, an expression for the probability of error is needed. The desired expression is:

$$P_E = \int \int_{R: \underline{\ell}_1 - \underline{\ell}_2 \geq 0} f(\underline{\ell}_1, \underline{\ell}_2|S_1) \cdot P(S_1) d\underline{\ell}_1, d\underline{\ell}_2 + \int \int_{R: \underline{\ell}_1 - \underline{\ell}_2 \leq 0} f(\underline{\ell}_1, \underline{\ell}_2|S_2) \cdot P(S_2) d\underline{\ell}_1 d\underline{\ell}_2 \quad (23)$$

where

P_E is the probability the receiver will make an error

P_i is the a priori probability that signal i is sent, equal to $\frac{1}{2}$ by assumption

Eq (23) reveals the need for knowledge of the joint statistics of the noise, to evaluate the performance of the receiver. In the special case of white Gaussian noise, the joint densities can be found from the first order density. ARN is not white or Gaussian, thus, knowledge of the higher order statistics is required to compute the performance of a known receiver.

Specification of the Optimal Binary Receiver. The first step in finding the optimal receiver is to select a cost function (Ref 29:24-26). In this section, the minimum probability of error is used as the cost function. The next step is to represent the received random process as a random vector. A convenient method for expanding the process for a finite observation interval employs the Karhunen-Loève expansion (Ref 29:174-209) to arrive at a truncated N dimensional representation involving random vectors where N is finite.

Now that the cost criterion is determined and the received random process is expressed in terms of a finite random vector, the only task left is to determine the decision region in the N dimensional decision space that will minimize the cost of the decision. This procedure is developed in many textbooks (Refs 29:25-27; 13:62-65). Eq (24) presents the decision rule that will minimize the probability of error of the decision for a binary receiver.

$$\frac{f(\tilde{R}|S_1)}{f(\tilde{R}|S_2)} \underset{S_0}{\overset{S_1}{>}} \frac{P_0}{P_1} \quad (24)$$

where

P_i = the a priori probability of transmitting signal S_i

$\bar{\mathbf{R}}$ = the received vector $(\mathbf{r}_1, \mathbf{r}_2, \dots, \mathbf{r}_N)$

$f(\bar{\mathbf{R}}|S_i)$ is the joint conditional density on $\bar{\mathbf{R}}$ assuming
 S_i is sent

The ratio of the two densities is known as the likelihood ratio.

Eq (24) specifies the computation that must be made by the optimal binary receiver. It should be noted that joint conditional densities are required to make the decision. Again for the case of white Gaussian noise, the joint densities can be determined from the first order densities. For ARN the joint densities cannot be determined from the lower order densities, thus the joint densities must be explicitly known.

Inadequacies of the Empirical Noise Models. The usefulness of empirical noise models is severely limited because they are only capable of representing the first order density function of the noise at the output of an envelope detector, as shown in Figure 5. The previous two sections demonstrate that joint density functions are required to evaluate the performance of an existing receiver and to specify the optimal receiver for a given noise environment.

There is no way to solve the optimal receiver problem using empirical noise models, but an approximation to the performance of a known receiver can be solved. This is accomplished by finding marginal densities on the quadrature components of the ARN, assuming the signal and noise are

statistically independent, and the random variables ℓ_1 and ℓ_2 , Figure 16, are statistically independent. The union bound is then used to find an upper limit on the probability of error (Refs 19; 33:264-265). This method is only marginally adequate for producing performance bounds (Ref 19). The union bound is only tight for certain conditions, but the real problem in using the union bound is in the assumption that the two random variables ℓ_1 and ℓ_2 are statistically independent.

One way to find the joint probability densities of the noise is to find a random process that represents the noise at the input to the receiver. If the noise is represented as a random process then it is theoretically possible to find all of the densities of the noise, and to determine the effect of the noise at different points in the receiver. This makes it possible to specify the optimal receiver and evaluate the exact performance of existing receivers. A process noise model is proposed and evaluated against the measured APD curves in the next chapter.

IV. A Random Point Process Model for ARN

Higher order statistics of the ARN cannot be found from empirical models. Therefore, a different type of noise model must be found. If the ARN is modeled as a random process, then it may be possible to completely characterize the process by finding all of its higher order joint density functions.

The model developed in this chapter is based on the mechanisms causing ARN. The proposed noise process is passed through an envelope detector receiver as in Figure 5; the output of the receiver is then compared to measured APD curves using plots and the fit parameter MSE. If the measured and theoretical APD curves match, then it is assumed higher order statistics produced by the model are also representative of ARN since the model is based on the physics causing the noise.

Development of the Noise Model

Lightning discharges are discrete events. Thus it is reasonable to use a random process with discrete event times to model the noise. The amplitude of the interference depends on the magnitude and location of the discharges. As pointed out in Chapter II, the most important discharge for VLF applications is the return stroke. Although return strokes

are often not independent of each other, they will be assumed statistically independent to preserve simplicity in the model. The Poisson process is a discrete random process (point process) that has independent event times (points). A point process must meet the following three conditions for it to be Poisson: (1) two events cannot occur at exactly the same time, (2) the occurrence of a point does not depend on previous points, and (3) there is no finite interval in which points occur with certainty (Ref 26:38-43). The Poisson process not only fulfills the requirement of independent event times, but also produces many analytically tractable results, and enjoys a rich theoretical development (Ref 26).

Empirical models such as the power-Rayleigh and Beckman's assume the noise has two components, one impulsive and the other a continuous background noise. Because of the close fitting APD curves produced by these models it is believed the proposed point process model must account for background noise. Other process models have been proposed using the sum of a Poisson and a Gaussian process (Refs 9; 23; 25). These models are moderately successful in producing APD curves that match measured curves, but the resulting processes are not analytically tractable. Therefore, the model proposed in this paper uses a second Poisson process with a high rate to account for the background noise. The high rate Poisson process has approximately the same effect

on a linear system as the Gaussian process used in other models. This occurs because a filtered Poisson process asymptotically tends to a Gaussian process as the rate approaches infinity or the bandwidth of the filter approaches zero (Ref 22:157). Thus the model proposed in this paper is the sum of two Poisson processes.

The magnitude of the interference seen at the receiver differs with each lightning stroke. Thus the magnitude of the points must be considered to be random variables. The magnitude of the points are referred to as marks by Snyder (Ref 26:128). When a Poisson process is marked it is called a compound Poisson process (Refs 22:128; 29:129). Since it is hypothesized the background noise originates from many distant storms it is reasonable to assume, because of the central limit theorem, that the marks are zero-mean Gaussian random variables. The highly impulsive part of the noise is caused by nearby storm activity. Since it is likely that more than one nearby lightning strike occurs in a given interval of time, and since there may be spatial correlation between the sites of stroke activity for nearby storms, the contribution from strokes may arrive with similar phases to produce a non-zero mean component to the noise process. Hence, the marks associated with the highly impulsive part of the noise model are assumed to be non-zero mean Gaussian random variables.

The resulting atmospheric radio noise model is

$$n(t) = \sum_{i=-\infty}^{\infty} a_i \delta(t-t_i) + \sum_{k=-\infty}^{\infty} b_k \delta(t-\mu_k) \quad (25)$$

where

t_i and μ_k are Poisson event times with different Poisson rates

a_i are i.i.d. Gaussian random variables $N_G(0, \sigma_1^2)$
(These are the high rate marks)

b_k are i.i.d. Gaussian random variables $N_G(m_2, \sigma_2^2)$
(These are the low rate marks)

$\delta(\cdot)$ is the Dirac-delta

$N_G(m, \sigma^2)$ specifies the mean and variance of a Gaussian random variable

The probability of observing n_1 Poisson events in an interval of T seconds is

$$P[N_{T1} = n_1] = \frac{(\lambda_1 T)^{n_1} \text{EXP}[-\lambda_1 T]}{n_1!} \quad (26)$$

where

λ_1 is the average rate of the high rate Poisson process with units of events per second

Similarly, the probability of observing n_2 Poisson events in an interval of T seconds is

$$P[N_{T2} = n_2] = \frac{(\lambda_2 T)^{n_2} \text{EXP}[-\lambda_2 T]}{n_2!} \quad (27)$$

where

λ_2 is the average rate of the low rate Poisson process with units of events per second

Verification of the Process Model

In this chapter the effect of the proposed noise process on the receiver shown in Figure 5 is examined. If the noise at the output of the receiver produces a match to the measured APD curves, the model accurately represents ARN, with respect to its first order density, and is assumed to also represent the higher order densities. Figure 18 shows a mathematical approximation to the envelope detector receiver used in the CCIR Report 322 measurements. This representation of the receiver is used to evaluate the accuracy of the proposed process model.

This model for the receiver uses quadrature multipliers and lowpass filters to represent the bandpass filter (Ref 33:496-501). The lowpass filter should have the same bandwidth as the bandpass filter. The bandpass filter is an ideal filter with a double sided bandwidth of 200 Hz. Thus the lowpass filter shown in Figure 18 should be an ideal lowpass filter with a single sided bandwidth of 100 Hz. An ideal lowpass filter can be approximated by an integrator. The frequency response of such an integrator is given by Eq (28).

$$H(f) = \frac{T \sin \pi f T}{\pi f T} \quad (28)$$

where

T is the integration time

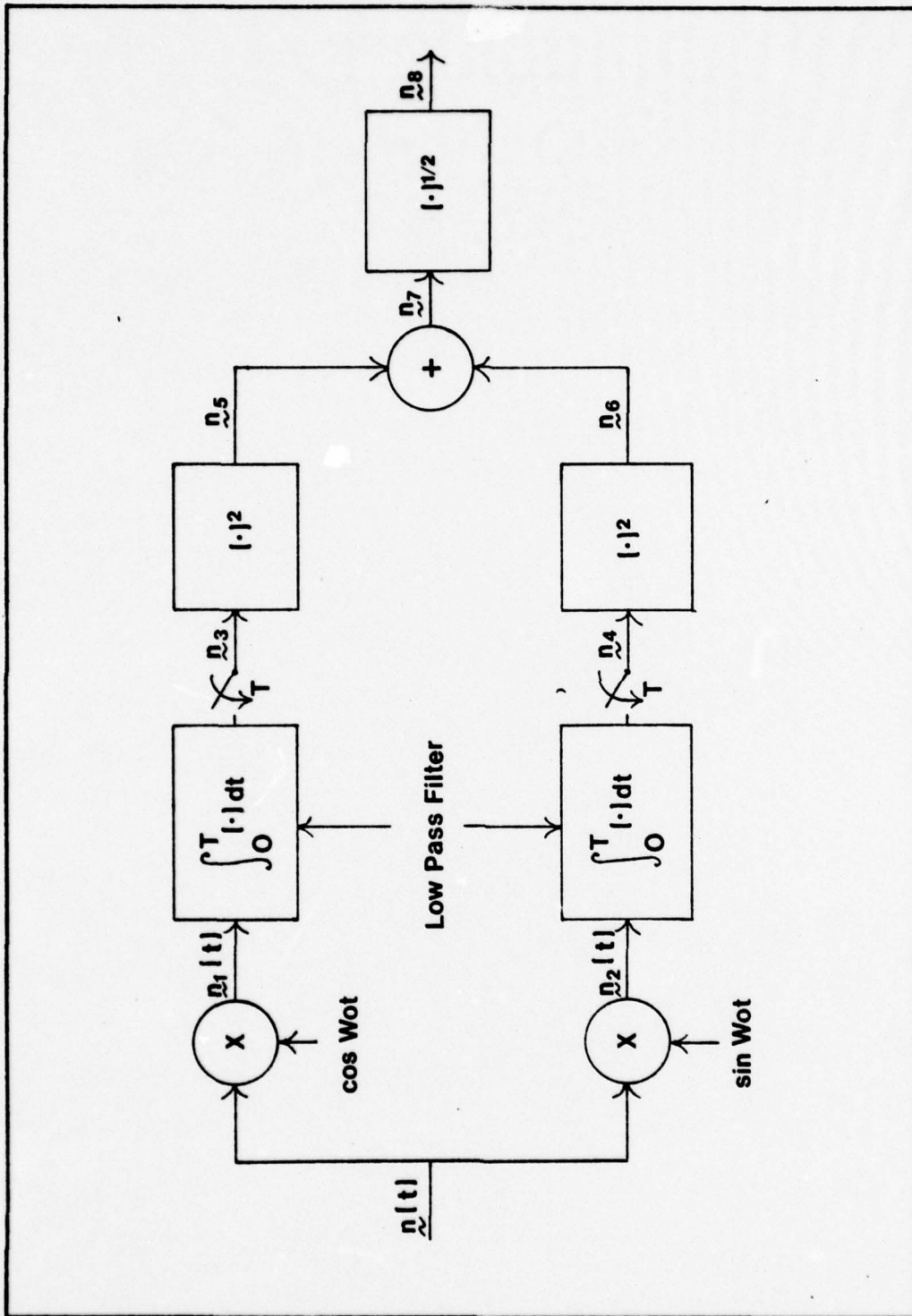


Figure 18. Mathematical Representation of CCIR Report 322 Receiver

The frequency response of Eq (28) can be made to approximate the ideal lowpass filter by selecting T so the first zero of the frequency response is equal to the bandwidth of the low-pass filter.

$$H(100) = 0 = \frac{T \sin\pi(100)T}{\pi(100)T} \quad (29)$$

Solving Eq (29) for T results in T = .01 seconds.

The receiver first multiplies $\underline{n}(t)$, the input noise process, by $\sin\omega_0 t$ and $\cos\omega_0 t$ where ω_0 is the center frequency of the bandpass filter.

$$\underline{n}_1(t) = \underline{n}(t)\cos\omega_0 t \quad (30)$$

$$\underline{n}_2(t) = \underline{n}(t)\sin\omega_0 t \quad (31)$$

where

$\underline{n}_1(t)$ and $\underline{n}_2(t)$ are shown in Figure 18.

The outputs of the integrators are

$$\underline{n}_3 = \int_0^T \underline{n}(t)\cos(\omega_0 t)dt \quad (32)$$

$$\underline{n}_4 = \int_0^T \underline{n}(t)\sin(\omega_0 t)dt \quad (33)$$

Using Eqs (25), (32), and (33) yields

$$\underline{n}_3 = \int_0^T \left[\sum_{i=-\infty}^{\infty} a_i \delta(t-t_i) \cos\omega_0 t + \sum_{k=-\infty}^{\infty} b_k \delta(t-t_k) \cos\omega_0 t \right] dt \quad (34)$$

$$n_4 = \int_0^T \left[\sum_{i=-\infty}^{\infty} a_i \delta(t-t_i) \sin \omega_0 t + \sum_{k=-\infty}^{\infty} b_k \delta(t-t_k) \sin \omega_0 t \right] dt \quad (35)$$

This reduces to

$$n_3 = \sum_{i=1}^{N_{T1}} a_i \cos \omega_0 t_i + \sum_{k=1}^{N_{T2}} b_k \cos \omega_0 t_k \quad (36)$$

and

$$n_4 = \sum_{i=1}^{N_{T1}} a_i \sin \omega_0 t_i + \sum_{k=1}^{N_{T2}} b_k \sin \omega_0 t_k \quad (37)$$

where

N_{T1} and N_{T2} are given by Eqs (26) and (27).

Squaring n_3 and n_4 produces n_5 and n_6 , respectively.

$$n_5 = \left[\sum_{i=1}^{N_{T1}} a_i \cos \omega_0 t_i + \sum_{k=1}^{N_{T2}} b_k \cos \omega_0 t_k \right]^2 \quad (38)$$

$$n_6 = \left[\sum_{i=1}^{N_{T1}} a_i \sin \omega_0 t_i + \sum_{k=1}^{N_{T2}} b_k \sin \omega_0 t_k \right]^2 \quad (39)$$

Eqs (38) and (39) become

$$\begin{aligned}
 n_5 = & \sum_{i=1}^{N_{T1}} \sum_{j=1}^{N_{T1}} a_i a_j \cos \omega_0 t_i \cos \omega_0 t_j \\
 & + 2 \sum_{i=1}^{N_{T1}} \sum_{k=1}^{N_{T2}} a_i b_k \cos \omega_0 t_i \cos \omega_0 t_k \\
 & + \sum_{k=1}^{N_{T2}} \sum_{j=1}^{N_{T2}} b_k b_j \cos \omega_0 t_j \cos \omega_0 t_j \quad (40)
 \end{aligned}$$

$$\begin{aligned}
 n_6 = & \sum_{i=1}^{N_{T1}} \sum_{j=1}^{N_{T1}} a_i a_j \sin \omega_0 t_i \sin \omega_0 t_j \\
 & + 2 \sum_{i=1}^{N_{T1}} \sum_{k=1}^{N_{T2}} a_i b_k \sin \omega_0 t_i \sin \omega_0 t_k \\
 & + \sum_{k=1}^{N_{T2}} \sum_{j=1}^{N_{T2}} b_k b_j \sin \omega_0 t_k \sin \omega_0 t_j \quad (41)
 \end{aligned}$$

n_7 is then given by the sum of n_5 and n_6 .

$$\begin{aligned}
n_7 = & \sum_{i=1}^{N_{T1}} \sum_{j=1}^{N_{T1}} a_i a_j \cos \omega_0 (t_i - t_j) \\
& + 2 \sum_{i=1}^{N_{T1}} \sum_{k=1}^{N_{T2}} a_i b_k \cos \omega_0 (t_i - \mu_k) \\
& + \sum_{k=1}^{N_{T2}} \sum_{j=1}^{N_{T2}} b_k b_j \cos \omega_0 (\mu_k - \mu_j) \quad (42)
\end{aligned}$$

n_8 is then obtained by taking the square root of n_7 .

To find the first order density function on the random variable n_7 or n_8 is a formidable task. However, insight about the first order density may be gained by observing n_3 and n_4 are conditionally Gaussian. n_3 and n_4 are the sum of independent Gaussian random variables when all t_i , t_k , N_{T1} , and N_{T2} are known.

The conditional densities on n_3 and n_4 are given below.

$$\begin{aligned}
f(n_3 | N_{T1} = N_1; N_{T2} = N_2, \bar{t}_i = \bar{t}_i, \bar{\mu}_k = \bar{\mu}_k) \\
= N_G \left(m \sum_{k=1}^{N_2} \cos \omega_0 \mu_k, \sigma_1^2 \sum_{i=1}^{N_1} \cos^2 \omega_0 t_i + \sigma_2^2 \sum_{k=1}^{N_2} \cos^2 \omega_0 \mu_k \right) \quad (43)
\end{aligned}$$

$$f(\underline{n}_4 | \underline{N}_{T1} = N_1, \underline{N}_{T2} = N_2, \bar{t}_i = \bar{t}_i, \bar{\mu}_k = \bar{\mu}_k) = N_G \left(m \sum_{k=1}^{N_2} \sin \omega_0 \mu_k, \sigma_1^2 \sum_{i=1}^{N_1} \sin^2 \omega_0 t + \sigma_2^2 \sum_{k=1}^{N_2} \sin^2 \omega_0 \mu_k \right) \quad (44)$$

where

\bar{t}_i and $\bar{\mu}_k$ are random vectors of event times

This results in the random variables \underline{n}_5 and \underline{n}_6 being distributed conditionally as non-central chi-squared (Ref 16:143). Thus, the random variable \underline{n}_7 is conditionally the sum of two non-central chi-squared random variables. From Eqs (43) and (44) it is seen that \underline{n}_3 and \underline{n}_4 are not conditionally identically distributed because of the $\sin \omega_0 t_i$ and $\cos \omega t_i$ terms. Thus, the random variables \underline{n}_5 and \underline{n}_6 are also not conditionally identically distributed. The random variables \underline{n}_3 and \underline{n}_4 may become conditionally i.i.d. when averaged over the possible values of \bar{t}_i , and $\bar{\mu}_k$. Thus, it is assumed \underline{n}_3 and \underline{n}_4 are in fact conditionally i.i.d. Gaussian random variables where the conditioning is with respect to \underline{N}_{T1} and \underline{N}_{T2} only. This means the conditional densities on \underline{n}_5 and \underline{n}_6 are i.i.d. non-central chi-square with one degree of freedom. Thus the conditional density on \underline{n}_7 is non-central chi-square with two degrees of freedom.

Using the assumption of conditionally i.i.d. Gaussian random variables reduces Eqs (36) and (37) to

$$\underline{n}_3 = \frac{1}{\sqrt{2}} \sum_{i=1}^{\underline{N}_{T1}} a'_i + \frac{1}{\sqrt{2}} \sum_{i=1}^{\underline{N}_{T2}} b'_k \quad (45)$$

$$\tilde{n}_4 = \frac{1}{\sqrt{2}} \sum_{i=1}^{N_{T2}} \tilde{a}_i'' + \frac{1}{\sqrt{2}} \sum_{i=1}^{N_{T2}} \tilde{b}_k'' \quad (46)$$

where

\tilde{a}_i' and \tilde{a}_i'' are i.i.d. Gaussian random variables

\tilde{b}_k' and \tilde{b}_k'' are i.i.d. Gaussian random variables

The $1/\sqrt{2}$ is a result of the cosine and sine terms in Eqs (35) and (36). The conditional probability density function on \tilde{n}_3 and \tilde{n}_4 from Eqs (45) and (46) are

$$\begin{aligned} f(\tilde{n}_3 | N_{T1} = N_1, N_{T2} = N_2) \\ = N_G(\sqrt{2} m_2 N_2, 2\sigma_1^2 N_1 + 2\sigma_2^2 N_2) \end{aligned} \quad (47)$$

$$\begin{aligned} f(\tilde{n}_4 | N_{T1} = N_1, N_{T2} = N_2) \\ = N_G(\sqrt{2} m_2 N_2, 2\sigma_1^2, N_1 + 2\sigma_2^2 N_2) \end{aligned} \quad (48)$$

Thus \tilde{n}_3 and \tilde{n}_4 are i.i.d. conditionally Gaussian random variables. Squaring \tilde{n}_3 and \tilde{n}_4 produces \tilde{n}_5 and \tilde{n}_6 which are conditionally independent non-central chi-squared random variables with one degree of freedom (Ref 16:147). Since \tilde{n}_5 and \tilde{n}_6 are i.i.d., their sum, \tilde{n}_7 , is a non-central chi-squared random variable with two degrees of freedom (Ref 17). This density is given by Eq (49).

$$f(n_7 | N_1, N_2) = \frac{1}{4(N_1\sigma_1^2 + N_2\sigma_2^2)} \cdot \text{EXP} \left[- \frac{n_7 + 4N_2^2 m_2^2}{4(N_1\sigma_1^2 + N_2\sigma_2^2)} \right] \\ \cdot I_0 \left[\frac{(n_7 N_2^2 m_2^2)^{\frac{1}{2}}}{N_1\sigma_1^2 + N_2\sigma_2^2} \right] \quad (49)$$

where

$I_0(\cdot)$ is the zero order modified Bessel function.

The joint density on n_7 , N_{T1} and N_{T2} can be found by combining Eqs (26), (27) and (49).

$$f(n_7, N_{T1}, N_{T2}) = f(n_7 | N_1, N_2) \cdot f(N_{T1} = N_1) \cdot f(N_{T2} = N_2) \quad (50)$$

The marginal density on n_7 can then be found by summing Eq (50) over all values of N_1 and N_2 .

$$f(n_7) = \sum_{N_1=0}^{\infty} \sum_{N_2=0}^{\infty} \frac{1}{4(N_1\sigma_1^2 + N_2\sigma_2^2)} \cdot \text{EXP} \left[- \frac{n_7 + 4N_2^2 m_2^2}{4(N_1\sigma_1^2 + N_2\sigma_2^2)} \right] \\ \cdot I_0 \left[\frac{(n_7 N_2^2 m_2^2)^{\frac{1}{2}}}{N_1\sigma_1^2 + N_2\sigma_2^2} \right] \cdot \frac{(\lambda_1 T)^{N_1} \text{EXP}(-\lambda_1 T)}{N_1!} \\ \cdot \frac{(\lambda_2 T)^{N_2} \text{EXP}(-\lambda_2 T)}{N_2!} \quad (51)$$

where

λ_1 and λ_2 are the high and low rates of the Poisson processes

T is the integration time (.01 seconds)

$$n_7 \geq 0$$

The first order density on n_8 can now be found by a simple transformation

$$n_8 = (n_7)^{\frac{1}{2}} \quad (52)$$

where

$$n_7 \geq 0$$

This produces

$$f(n_8) = \sum_{N_1=0}^{\infty} \sum_{N_2=0}^{\infty} \frac{n_8}{2(N_1\sigma_1^2 + N_2\sigma_2^2)} \cdot \text{EXP} \left[- \frac{n_8^2 + 2N_2 m_2^2}{4(N_1\sigma_1^2 + N_2\sigma_2^2)} \right] \\ \cdot I_0 \left[\frac{n_8 N_2 m_2}{N_1\sigma_1^2 + N_2\sigma_2^2} \right] \cdot \frac{(\lambda_1 T)^{N_1} \text{EXP}(-\lambda_1 T)}{N_1!} \\ \cdot \frac{(\lambda_2 T)^{N_2} \text{EXP}(-\lambda_2 T)}{N_2!} \quad (53)$$

where

$$n_8 \geq 0$$

This is approximately the resulting density of the noise measured at the output of a receiver such as the one used by Crichlow.

The result of Eq (53) is now compared to the measured APD curves from CCIR Report 322. The first step in comparing the curves is to find the proper parameters, λ_1 , λ_2 , m_2 , σ_1^2 , σ_2^2 . This is done by numerically differentiating the measured APD curves to obtain a first order density of the measured noise. Parameters are then selected for use in Eq (53) by using a gradient search subroutine to adjust the parameters to minimize the mean-square error in fit between the two curves when plotted on a logarithmic scale. The gradient search routine used is ZXMIN found in the IMSL library. The logarithmic scale is used because of the large dynamic range of the density curves. The density curves are used for finding parameters instead of the APD curves because of computational considerations. If the fit between the APD curves is used to find the parameters, then Eq (53) would have to be integrated thousands of times during the gradient search procedure. This is not feasible in terms of computer time.

Table I contains the parameters obtained by the above procedure. Eq (53) must now be numerically integrated using the parameters in Table I to obtain values for the APD curves. The numerical integration that must be performed is shown in Eq (54).

$$P(\underline{n}_g > n) = 1 - \int_0^n f(\underline{n}_g) d\underline{n}_g \quad (54)$$

Table I
Parameters for the Point Process Model

Parameter	$V_d = 4$	$V_d = 10$
λ_1	300	500
λ_2	10	30
σ_1^2	.019	.0005
σ_1^2	25	5
m_2	.08	.85

where

η is the threshold represented on the abscissa of Crichlow's APD curves

The resulting curves and values of MSE for V_d ratios of 4 and 10 are shown in Figures 19 and 20.

The curves show close agreement between measured and theoretical APD curves for both low and high probability of exceedence. The theoretical data points are found to deviate a sizable amount from the measured curve for mid-range values of probability of exceedence. This is thought to be caused by the use of a logarithmic scale when matching the density curves. This causes parameters to be selected that produce an excellent fit in the tail sections of the density but not as close a fit for the larger valued section near $\Delta = 0$. The values of MSE are almost as good as for Beckman's model

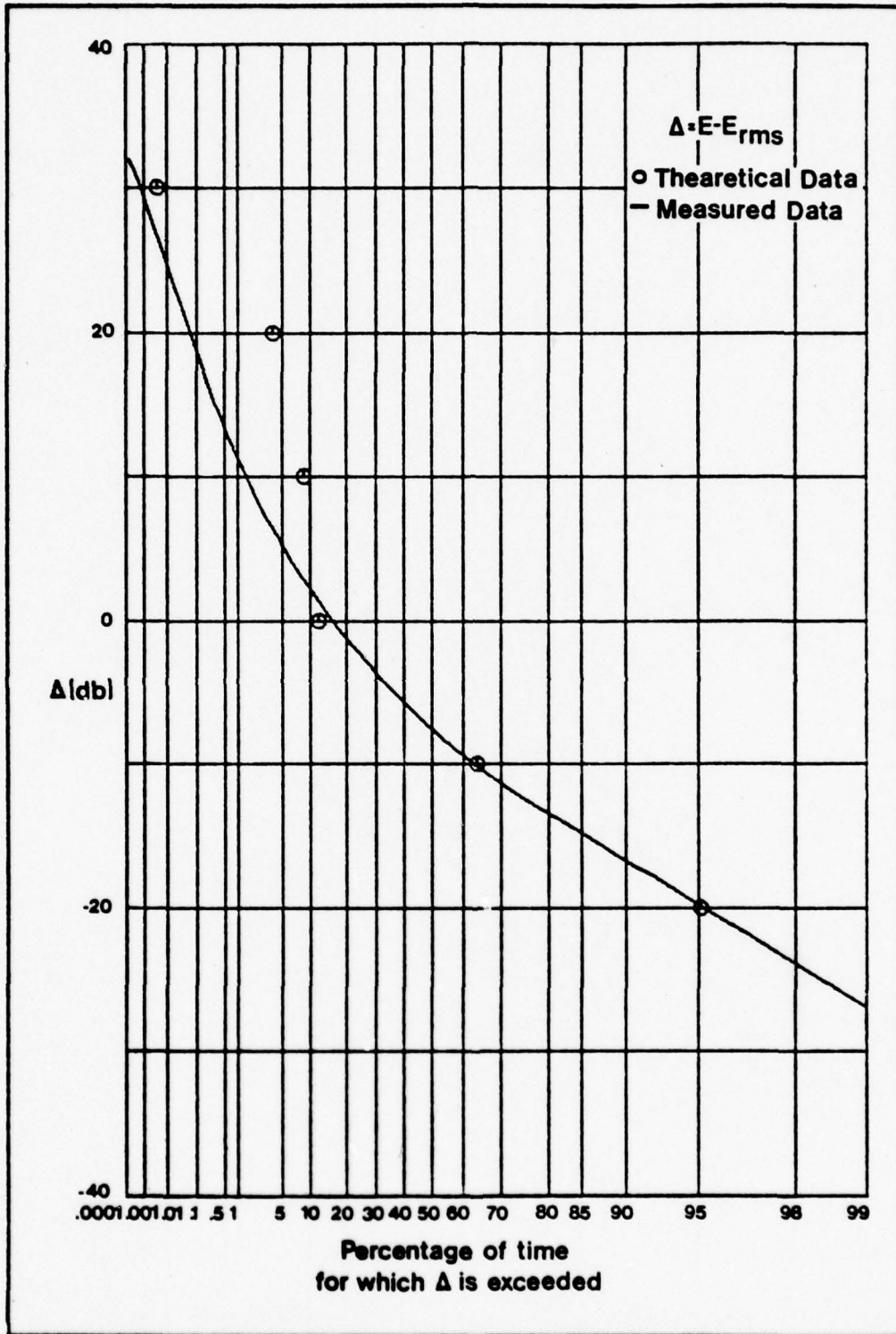


Figure 19. Comparison of Measured and Process Model APD Curves, $V_d = 4$ (MSE = .00958)

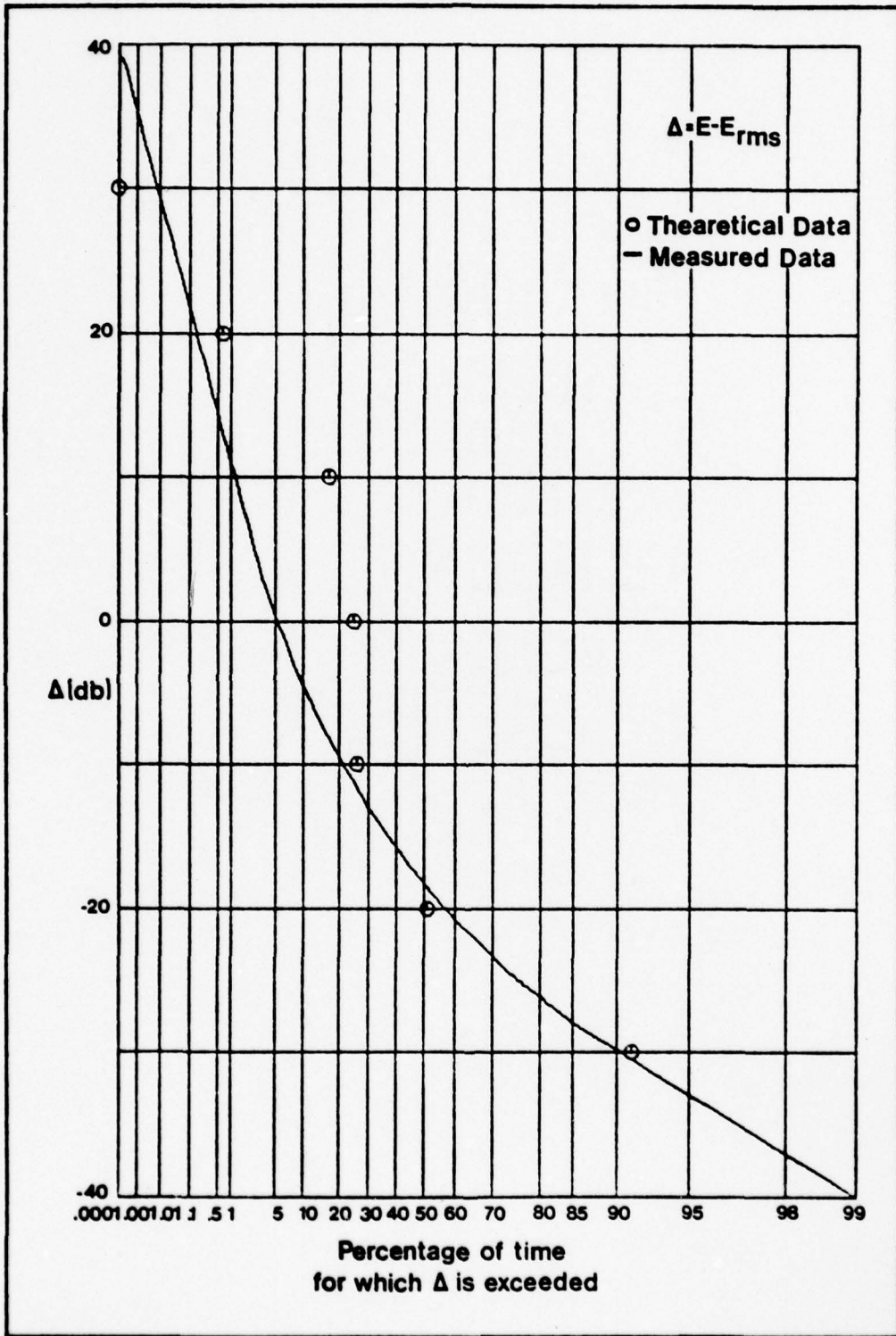


Figure 20. Comparison of Measured and Process Model APD Curves, $V_d = 10$ (MSE = .0357)

and are much better than for the mixture model. This results because of the high accuracy of the high and low probability of exceedence values on the APD curves. Thus, this special case of the process model fits the measured APD curves, in terms of MSE, almost as well as the Beckman model.

V. Conclusions

Existing empirical noise models are not adequate for evaluating the performance of known receiver structures or specifying the structure of the optimal receiver in atmospheric radio noise. While all but one of the empirical models examined in Chapter II results in an analytical expression that closely matches the measured APD curves in CCIR Report 322, none of the models contain any information about the higher order density functions of the noise. The higher order densities are required to evaluate the performance of known receivers and specify the optimal receiver. Thus, empirical noise models are of limited use to communication engineers.

Modeling the atmospheric radio noise as a random process allows higher order densities to be found. If the higher order statistics are to be representative of ARN, then the process must be based on the physics causing ARN. Thus, the noise model proposed in Chapter IV is based on the physical processes causing ARN.

Under certain assumed restrictions the model described in Chapter IV produces APD curves that fit the measured APD curves of CCIR Report 322 with less than five percent mean-square error. Thus, the proposed random point process model adequately represents the first order statistics of

atmospheric radio noise. Since the proposed model is based on the underlying physical processes causing ARN, the higher order densities resulting from the model are also representative of ARN.

This process model is used to obtain an approximate expression for the first order density function of the noise present at the output of the receiver specified in CCIR Report 322. In principle, the exact expression for the first order density can be found. This warrants further investigation. If it can be shown that the exact expression also results in APD curves that closely approximate the measured curves, then the proposed model is definitely an accurate representation for at least the first order statistics of the noise. No measurements of higher order statistics of the noise exist; therefore, it is not possible to verify that higher order statistics agree. Using the higher order statistics from the model as an accurate representation of the higher order statistics of ARN, the performance of existing receivers can be studied and the optimal receiver structure can be specified.

Bibliography

1. Abromowitz, Milton and Irene A. Stegun. Handbook of Mathematical Functions. New York: Dover Publication, Inc., 1972.
2. Beach, C. D. and D. C. George. Error Performance of VLF and LF Receiving Systems with Nonlinear Atmospheric Noise Reduction. Contract F30602-69-C-0057. Boulder, Colorado, NBS, 1970.
3. Beckman, Petr. "Amplitude-Probability Distribution of Atmospheric Radio Noise," Radio Science Journal of Research, 68D (6):723-736 (June 1964).
4. Brooks, C. E. P. "The Distribution of Thunderstorms Over the Globe," Geophysics, 3:145-165 (1925).
5. Crichlow, W. Q., et al. Amplitude Probability Distributions for Atmospheric Radio Noise. National Bureau of Standards Monograph 23, PB183992. Washington, D. C.: Department of Commerce, November 1960.
6. _____. "Noise Investigation at VLF by the National Bureau of Standards," Proceedings of the IRE, 42:778-783 (June 1957).
7. _____. World Distribution and Characteristics of Radio Noise. CCIR Report 322. Geneva: International Telecommunication Union, 1964.
8. Field, Edward C., Jr. and Marcies Lewinstein. "Amplitude-Probability Distribution Model for VLF/ELF Atmospheric Noise," IEEE Transactions on Communications, Com-26 (1):1978.
9. Furutsu, K. and T. Ishida. "On the Theory of Amplitude Distribution of Impulsive Random Noise," Journal of Applied Physics, 32 (7):1206-1221 (1963).
10. Gamble, John T. An Analysis of Linear and Non-Linear Coherent Detection in Atmospheric Noise at Very-Low Frequency. AD/A-002833. Griffis Air Force Base, New York: Rome Air Development Center, November 1974.
11. Giorando, A. Modeling of Atmospheric Noise. Ph.D. Dissertation, University Microfilms #70-25,651. University of Pennsylvania, 1970.

12. Hall, Harry M. A New Model for Impulsive Phenomena: Application to Atmospheric-Noise Communications Channels. AD/648650. Stanford, California: Stanford University, August 1966.
13. Hastings, N. A. J. and J. B. Peacock. Statistical Distributions. New York: John Wiley and Sons, Inc., 1975.
14. Helstrom, Carl W. Statistical Theory of Signal Detection. New York: Pergamon Press, 1960.
15. Horner, F. and J. Hawood. "An Investigation of Atmospheric Radio Noise at Very Low Frequencies," IEEE Proceedings, 103 (B):743-751 (1958).
16. Katz, Samuel. Continuous Univariate Distributions--2. Boston: Hought Mifflin Company, 1970.
17. McNolty, Frank. "A Contour-Integral Derivation of the Non-Central Chi-Squared Distribution," Annals of Mathematical Statistics, 33:796-800 (1962).
18. Nakagomi, Minoru. "The M-Distribution--A General Formula of Intensity Distribution of Rapid Fading," Statistical Methods of Radio Wave Propagation. Pergamon Press, 1960.
19. Nejezchleb, Allen L. Evaluation of Coherent FSK Performance in Atmospheric Radio Noise. MS Thesis. Wright-Patterson AFB, Ohio: Air Force Institute of Technology, December 1977.
20. Olsen, Kenneth R. Performance Analysis of Continuous-Phase-Frequency Shift Keying Modulation in Atmospheric Noise. MS Thesis. Wright-Patterson AFB, Ohio: Air Force Institute of Technology, December 1977.
21. Papoulis, Athanasios. Probability, Random Variables, and Stochastic Processes. New York: McGraw-Hill Book Company, 1965.
22. Parzen, Emanuel. Stochastic Processes. San Francisco: Holden-Day Inc., 1967.
23. Sankur, B. "Modelling and Analysis of Impulsive Noise," Proceedings of NATO Advanced Study Institute on Communications Systems and Random Processes Theory. August 1977.
24. Schonhoff, Thomas A. CPMFSK as a Modulation on the VLF-HF Atmospheric Channel. Preliminary report prepared for Rome Air Development Center. Syracuse, New York: GTE Sylvania Inc., July 1977.

25. Snyder, D. L. "Optimal Binary Detection of Known Signals in a Non-Gaussian Noise Resembling VLF Atmospheric Noise," Wescon Technical Papers, Session 6. August 1968.
26. _____ . Random Point Processes. New York: John Wiley and Sons, 1975.
27. Spaulding, A. D. "Conversion of the Amplitude-Probability Distribution of Atmospheric Radio Noise from One Bandwidth to Another," Journal of Research of National Bureau of Standards--D. Radio Propagation, 66D (6):713-720 (1962).
28. Uman, M. A. Lightning. New York: McGraw-Hill Book Company, 1969.
29. Van Trees, Harry L. Detection, Estimation and Modulation Theory, Part I. New York: John Wiley and Sons Inc., 1968.
30. Watt, A. D. "Measured Statistical Characteristics of VLF Atmospheric Radio Noise," Proceedings of the IRE, 45 (1): (1957).
31. Watt, A. D. VLF Radio Engineering. New York: Pergamon Press, 1967.
32. Wilson, Kenneth E. Analysis of the Crichlow Graphical Model of Atmospheric Radio Noise at Very Low Frequencies. MS Thesis. Wright-Patterson AFB, Ohio: Air Force Institute of Technology, November 1974. AD-A008679.
33. Wozencraft, John M. and Irwin M. Jacobs. Principles of Communication Engineering. New York: John Wiley and Sons Inc., 1965.

Appendix A

Beckman's Model for ARN

This section presents the information required to reproduce the results shown in Figures 13 and 15. This section explains how the Beckman model is derived and used. Some useful numerical approximations are also presented.

The Beckman model is the sum of two random vectors. Each vector has a magnitude and phase. The magnitude of the first vector is Rayleigh distributed while the second vector is lognormally distributed. Both vectors have uniform distribution of the phase component. R_1 is the Rayleigh magnitude, R_2 is the lognormal magnitude, and θ is the phase.

$$f_1(R_1, \theta) = \frac{R}{2\pi N_c} \text{EXP}\left[-\frac{R}{2N_c}\right] \quad (55)$$

$$f_2(R, \theta) = \frac{1}{\sigma R (2\pi)^{\frac{3}{2}}} \text{EXP}\left[-\frac{(\text{Ln}(R) - \sigma^2)^2}{2\sigma^2}\right] \quad (56)$$

where

σ^2 is the variance of the lognormal random variable

N_c is the variance of the Rayleigh random variable

$\text{Ln}(\cdot)$ is the natural logarithm

Using the following transformation of random variable

$$R^2 = X^2 + Y^2$$

$$\theta = \tan^{-1}\left(\frac{Y}{X}\right)$$

and Eqs (55) and (56) produces the following densities on the Rayleigh and lognormal vectors.

$$f_1(X, Y) = \frac{1}{2\pi N_c} \text{EXP}\left[-x \frac{X^2 + Y^2}{2N_c}\right] \quad (57)$$

$$f_2(X, Y) = \frac{1}{\sigma(X^2+Y^2)(2\pi)^{\frac{3}{2}}} \text{EXP}\left[-\frac{(\text{Ln}[(X^2+Y^2)^{\frac{1}{2}}] + \sigma^2)^2}{2\sigma^2}\right] \quad (58)$$

The Beckman model requires these two statistically independent vectors to be summed. The resulting density is given by the convolution of the density from Eqs (57) and (58).

$$f(X_o, Y_o) = \int_{-\infty}^{\infty} \int f_2(X, Y) \cdot f_1(X_o - X, Y_o - Y) dx dy \quad (59)$$

The result is

$$f(X_o, Y_o) = \int_{-\infty}^{\infty} \int \frac{1}{(2\pi)^{\frac{3}{2}} \sigma N_c (X^2+Y^2)} \text{EXP}\left[-\frac{(\text{Ln} (X^2+Y^2)^{\frac{1}{2}} + \sigma^2)^2}{2\sigma^2} - \frac{(X_o - X)^2 + (Y_o - Y)^2}{2N_c}\right] dx dy \quad (60)$$

Using the following transformation of random variable produces Eq (65)

$$X = R \cos\theta \quad (61)$$

$$Y = R \sin\theta \quad (62)$$

$$X_0 = R_0 \cos\theta \quad (63)$$

$$Y_0 = R_0 \sin\theta \quad (64)$$

$$f(R_0, \theta) = \int_0^{\infty} \frac{2R_0}{(2\pi)^{\frac{1}{2}} \sigma N_c R} \text{EXP} \left[- \frac{(\text{Ln}(R) + \sigma^2)^2}{2\sigma^2} - \frac{R_0^2 + R^2}{2Nc} \right] \\ \cdot \int_0^{\pi} \text{EXP} \left[\frac{R_0 R}{Nc} \cos\theta \right] d\theta dR \quad (65)$$

Using the definition of the zero order modified Bessel function (Ref 1:259) produces

$$f(R_0) = \int_0^{\infty} \frac{R_0}{(2\pi)^{\frac{1}{2}} \sigma N_c R} \text{EXP} \left[- \frac{(\text{Ln}(R) + \sigma^2)^2}{2\sigma^2} - \frac{R_0^2 + R^2}{2Nc} \right] \\ \cdot I_0 \left(\frac{RR_0}{Nc} \right) dR \quad (66)$$

Eq (66) is the result shown in Chapter III.

To calculate the data points found in Figures 13 and 15 requires integration of Eq (66). Eq (67) is an approximation to Eq (66) that can be used for $R > 12$ and $R_0 > 12$.

$$f(R_0) = \int_0^{\infty} \frac{R_0}{(2\pi)^{\frac{1}{2}} \sigma N_c R} \text{EXP} \left[- \frac{(\text{Ln}(R) + \sigma^2)^2}{2\sigma^2} - \frac{(R_0 - R)^2}{2Nc} \right] \quad (67)$$

The most difficult problem in using the Beckman model is finding the proper parameters, σ and N_c . A method for approximating these parameters from knowledge of the measured APD curves is now presented. The position of the Rayleigh straight line portion of the APD curve determines the value of N_c . This portion of the curve can be approximated by

$$P(R_o > R) = \text{EXP} \left[- \frac{R}{N_c} \right] \quad (68)$$

By reading the value of threshold, Δ , at which the APD curve crosses the .99 probability of exceedence point and using Eq (68) results in Eq (69)

$$N_c = - \frac{R^2}{\text{Ln}(.99)} \quad (69)$$

where

Ln is the natural logarithm

The value of σ can be determined from the slope of the (straight line) lognormal portion of the APD curve when plotted on Rayleigh probability paper (Ref 3:735). Figure 21 is a plot of slope versus σ . These methods of obtaining the parameters only produce approximate values, thus some adjustment of the values may be required to obtain the best fit to the measured data. The values of σ and N_c used in Figures 13 and 15 are $\sigma = 1.04$ and $N_c = .0973$ for V_d of 4 and $\sigma = 1.32$ and $N_c = .00985$ for V_d of 10.

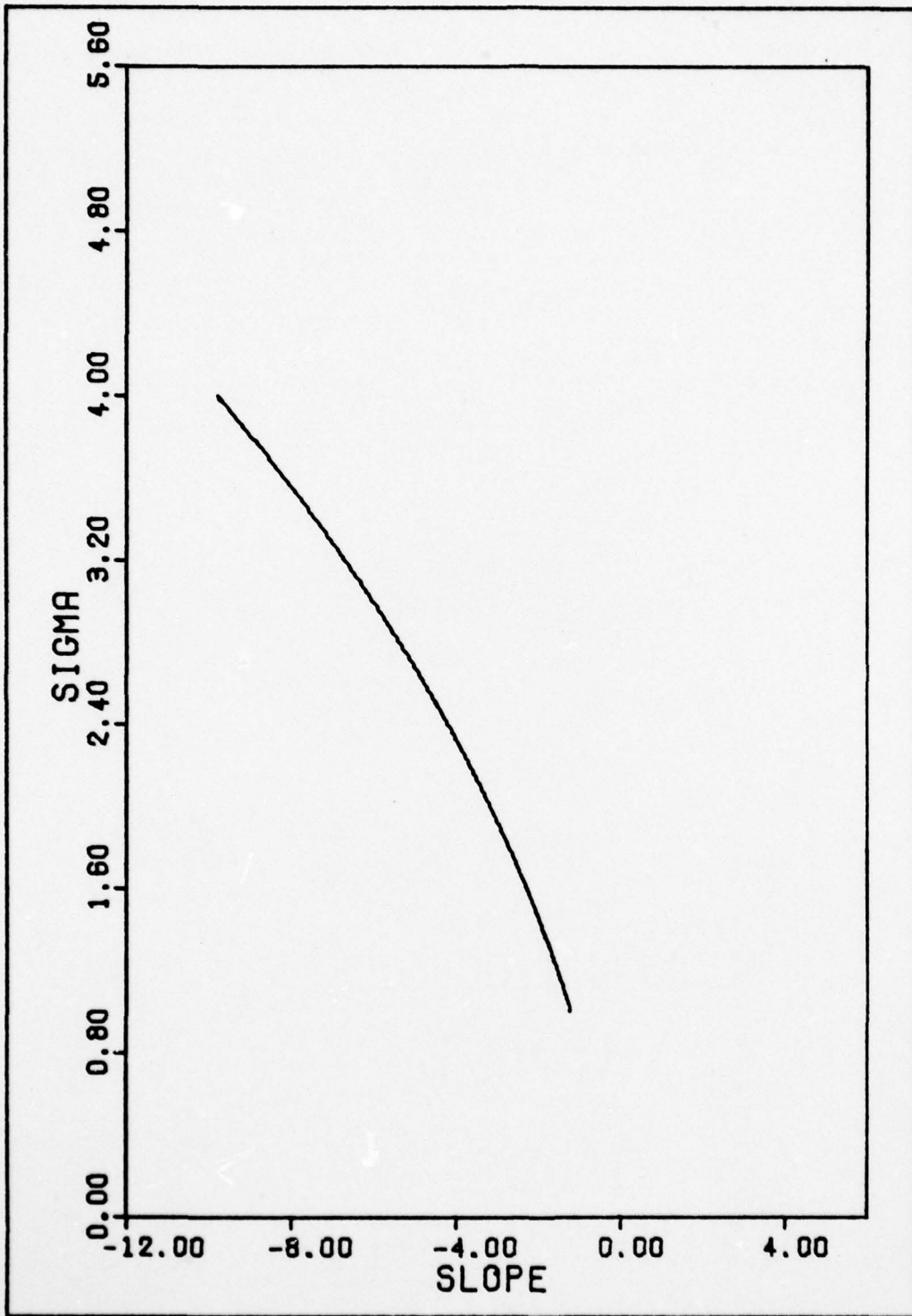


Figure 21. APD Curve Slope vs. σ from the Beckman Model

Vita

Steven D. Hettinger was born October 14, 1953, in Des Moines, Iowa. His family moved to Orange, California, in 1964, where he lived until graduating from high school. He then moved to San Diego, California, where he attended San Diego State University. He graduated with honors in electrical engineering, received a commission in the USAF, and was married in 1975. During his last two years of undergraduate school and the following year, while waiting to enter active duty, he worked for Naval Electronics Laboratory Center in San Diego. Upon entering active duty, he was stationed at the Air Force Institute of Technology at Wright-Patterson Air Force Base, Ohio.

Permanent address: 2888 Wyngate Road
Orange, California 92667

UNCLASSIFIED

SECURITY CLASSIFICATION OF THIS PAGE (When Data Entered)

REPORT DOCUMENTATION PAGE		READ INSTRUCTIONS BEFORE COMPLETING FORM
1. REPORT NUMBER AFIT/GE/EE/78-3	2. GOVT ACCESSION NO.	3. RECIPIENT'S CATALOG NUMBER
4. TITLE (and Subtitle) A RANDOM POINT PROCESS MODEL FOR ATMOSPHERIC RADIO NOISE	5. TYPE OF REPORT & PERIOD COVERED MS Thesis	
	6. PERFORMING ORG. REPORT NUMBER	
7. AUTHOR(s) Steven D. Hettinger 2nd Lt USAF	8. CONTRACT OR GRANT NUMBER(s)	
9. PERFORMING ORGANIZATION NAME AND ADDRESS Air Force Institute of Technology (AFIT-EN) Wright-Patterson AFB, Ohio 45433	10. PROGRAM ELEMENT, PROJECT, TASK AREA & WORK UNIT NUMBERS	
11. CONTROLLING OFFICE NAME AND ADDRESS	12. REPORT DATE March 1978	
	13. NUMBER OF PAGES 86	
14. MONITORING AGENCY NAME & ADDRESS (if different from Controlling Office)	15. SECURITY CLASS. (of this report) Unclassified	
	15a. DECLASSIFICATION/DOWNGRADING SCHEDULE	
16. DISTRIBUTION STATEMENT (of this Report) Approved for public release; distribution unlimited		
17. DISTRIBUTION STATEMENT (of the abstract entered in Block 20, if different from Report)		
18. SUPPLEMENTARY NOTES Approved for public release; IAW AFR 190-17 <i>J. F. Guess</i> JERRAL F. GUESS, Captain, USAF Director of Information		
19. KEY WORDS (Continue on reverse side if necessary and identify by block number) Atmospheric Radio Noise Very-Low Frequency Random Processes Noise Poisson Processes		
20. ABSTRACT (Continue on reverse side if necessary and identify by block number) The physical processes causing atmospheric radio noise in the very-low frequency communication channel are examined. The return strokes from lightning discharges are found to be the major source of the noise. A survey of empirical noise models is presented. The models are compared in terms of their ability to match the measured first order statistics from CCIR Report 322. While all of these models have advantages and disadvantages, it is observed		

UNCLASSIFIED

SECURITY CLASSIFICATION OF THIS PAGE(When Data Entered)

that all are inadequate to evaluate the performance of known receivers or to specify the optimal receiver structure. This results because empirical noise models give no information about the higher order statistics of the noise. A new model for atmospheric radio noise is developed. This model is a random process model that is based on the physical processes causing the noise. Higher order statistics of the noise can be determined, at least in principle, from this type of model. The model consists of the sum of two compound Poisson processes. The first order statistics from this model are compared to the measured statistics from CCIR Report 322. Based on this, the model is found to be a valid representation for atmospheric radio noise in the very-low frequency channel.

UNCLASSIFIED

SECURITY CLASSIFICATION OF THIS PAGE(When Data Entered)